FINITE ELEMENT IMPLEMENTATION OF A MODEL TO ESTIMATE THE PERMANENT STRAIN OF CYCLICALLY-LOADED SOIL

A THESIS SUBMITTED TO
THE GRADUATE SCHOOL OF NATURAL AND APPLIED SCIENCES
OF
MIDDLE EAST TECHNICAL UNIVERSITY

BY

MUHİTTİN BABAOĞLU

IN PARTIAL FULFILLMENT OF THE REQUIREMENTS
FOR
THE DEGREE OF MASTER OF SCIENCE
IN
CIVIL ENGINEERING

JULY 2020

Approval of the thesis:

FINITE ELEMENT IMPLEMENTATION OF A MODEL TO ESTIMATE THE PERMANENT STRAIN OF CYCLICALLY-LOADED SOIL

submitted by **MUHİTTİN BABAOĞLU** in partial fulfillment of the requirements for the degree of **Master of Science in Civil Engineering Department, Middle East Technical University** by,

Prof. Dr. Halil Kalıpçılar
Dean, Graduate School of **Natural and Applied Sciences** _____

Prof. Dr. Ahmet Türer
Head of Department, **Civil Engineering** _____

Prof. Dr. Sinan Turhan Erdoğan
Supervisor, **Civil Engineering, METU** _____

Assoc. Prof. Dr. H. Ercan Taşan
Co-supervisor, **Civil Engineering** _____

Examining Committee Members:

Prof. Dr. Özgür Yaman
Civil Engineering, METU _____

Prof. Dr. Sinan Turhan Erdoğan
Civil Engineering, METU _____

Prof. Dr. Berna Unutmaz
Civil Engineering, Hacettepe University _____

Prof. Dr. Zeynep Gülerce
Civil Engineering, METU _____

Assist. Prof. Dr. Onur Pekcan
Civil Engineering, METU _____

Date: 03.07.2020

I hereby declare that all information in this document has been obtained and presented in accordance with academic rules and ethical conduct. I also declare that, as required by these rules and conduct, I have fully cited and referenced all material and results that are not original to this work.

Name, Surname: Muhittin Babaoğlu

Signature :

ABSTRACT

FINITE ELEMENT IMPLEMENTATION OF A MODEL TO ESTIMATE THE PERMANENT STRAIN OF CYCLICALLY-LOADED SOIL

Babaoğlu, Muhittin
M.S., Department of Civil Engineering
Supervisor: Prof. Dr. Sinan Turhan Erdoğan
Co-Supervisor: Assoc. Prof. Dr. H. Ercan Taşan

July 2020, 76 pages

In vast majority of geotechnical structures such as monopile or strip foundation, which are subjected to repeated loading, long-term resilience of the structures is directly related with the behavior of granular materials subjected to cyclic loading. Repeatedly loaded structure distributes stress to soil that surrounds the structure. When granular materials are exposed to cyclic loading, plastic strain occurs despite the applied stress is less than plastic yield, which results to residual settlement. This thesis provides a simplified numerical method implementation in finite element method (FEM) that estimates deformation of granular materials exposed to high numbers of cyclic loading for intricate 3D systems. Using explicit approach, which determines permanent strain for a specific number of loading cycles by means of empirical formulas in one solution step, this method eliminates error accumulation due to every FEM steps. Required experimental tests to obtain model parameters are elaborated. This model is utilized for the simulation of constant-amplitude cyclic loaded monopile embedded in soil. Comparison of numerical results with experimental data indicates great agreement and considerable improvement over commonly used existed methods. This study offers suggestions for prospective researches in the view of proposed

method, which focus on 3D modeling of cyclic loaded granular materials. Furthermore, varying-amplitude cyclic loaded monopile is also modeled as an extension of the proposed model with strain-hardening approach.

Keywords: Permanent deformation, cyclic loading, granular materials, finite element method

ÖZ

TEKRARLI YÜKLENEN ZEMİNLERİN KALICI ŞEKİL DEĞİŞTİRMELERİNİ HESAPLAMAK İÇİN SONLU ELEMAN UYGULAMA MODELİ

Babaoğlu, Muhittin
Yüksek Lisans, İnşaat Mühendisliği Bölümü
Tez Yöneticisi: Prof. Dr. Sinan Turhan Erdoğan
Ortak Tez Yöneticisi: Doç. Dr. H. Ercan Taşan

Temmuz 2020 , 76 sayfa

Tekrarlı yüklere maruz kalan tekil kazık ya da sürekli temel gibi geoteknik yapıların uzun dönem dayanımı, taneli malzemelerin tekrarlı yükler altında davranışıyla doğrudan ilgilidir. Tekrarlı yüklere maruz kalan yapılar, üzerlerinde oluşan gerilimi etrafındaki zemine dağıtırlar. Uygulanan gerilme kalıcı oturmalara neden olan plastik akma seviyesinden az olsa dahi, taneli malzemeler tekrarlı yükler altında kalmaları halinde plastik şekil değiştirme gösterirler. Bu tez, yüksek sayıda tekrarlı yüke maruz kalmış kompleks üç boyutlu taneli malzemeli sistemlerin deformasyon tahmini için sonlu elemanlar yönteminde basitleştirilmiş numerik yöntem uygulaması sunmaktadır. Tek çözüm adımında ampirik formüller kullanarak yüksek sayıdaki tekrarlar için kalıcı şekil değiştirmeleri belirleyen açık yöntemlerin kullanılması, sonlu elemanlar yönteminin her adımında oluşan hata birikmesini engeller. Bu modelde kullanılan parametreleri elde etmek için gereken deneysel testler hakkında bilgi verilmiştir. Önerilen bu yöntem zemin içine saplanmış, sabit şiddetli tekrarlı yüklerle yüklenmiş tekli kazıkların simülasyonunda kullanılmıştır. Numerik ve deneysel sonuçların kıyaslaması iyi uyumlar göstermiş olup, mevcut yöntemlere kıyasla gelişme kat edilmiştir.

Bu çalışma, tekrarlı yükler uygulanan taneli malzemelerin üç boyutlu modellemesi için önerilen bu yöntem ışığında, gelecek çalışmalar için tavsiyelerde bulunmaktadır. Buna ek olarak, değişken şiddetli tekrarlı yüklerle yüklenen tekli kazıklar, mevcut yönteme bir ek olarak şekil değiştirme sertleşmesi yöntemiyle de modellenmiştir.

Anahtar Kelimeler: Kalıcı deformasyon, tekrarlı yükler, taneli malzemeler, sonlu eleman yöntemi

To my family

ACKNOWLEDGMENTS

First and foremost, I would like to express my greatest appreciation to my thesis supervisor Prof. Dr. Sinan T. Erdoğan, for his contribution to both my thesis and my academic development. Apart from being an academic supervisor, his constant support, precious recommendations, and guidance throughout my thesis are tremendously significant. I am obliged to express my sincere gratitude to my co-supervisor, Assoc. Prof. Dr. H. Ercan Taşan, for his support during my master's thesis. His instrumental assistance, expertise, and encouragement during the thesis are invaluable. I consider myself lucky for I had benefitted from their mentorship during this process.

Moreover, I am thankful for my thesis committee members, Dr. Özgür Yaman, Dr. Berna Unutmaz, Dr. Zeynep Gülerce and Dr. Onur Pekcan for their valuable comments and guidance on my research.

Among the faculty members of the Konya Technical University (KTUN) Civil Engineering Department, I sincerely feel in dept to thank my deceased advisor in KTUN, Prof. Dr. Özcan Tan, for his support throughout the master thesis. I am deeply sorry for his sudden loss, but his kindness and assistance will always be honored and remembered. Furthermore, I would like to thank all members and colleagues of the KTUN Geotechnics division for their understanding during the process.

I would like to thank my dear friend Aykut Bilginer for the great help, and also, my friends Fırat Dal and Berkay Akçören for their support during CE 4006 & CE 7018.

Mostly, I am indebted to thank my father and all of my dear family for their endless support and encouragement throughout my life. And in the end, I owe it all to my wife Gözde, for always being there for me in my decisions.

TABLE OF CONTENTS

ABSTRACT v

ÖZ vii

ACKNOWLEDGMENTS x

TABLE OF CONTENTS xi

LIST OF TABLES xv

LIST OF FIGURES xvi

LIST OF ABBREVIATIONS xix

CHAPTERS

1 INTRODUCTION 1

1.1 Problem Definition and Motivation 2

1.2 Outline of Thesis 3

2 A SURVEY OF COMPUTATIONAL MODELING OF GRANULAR MATERIALS 5

2.1 Brief Timeline of Granular Materials Constitutive Modeling 5

2.2 Application of the Finite Element Method in Granular Materials . . . 6

2.3 Laws of Conservation 7

2.3.1 Internal Energy in Solids 8

2.4 Material Equation 9

2.5 Weak Form 11
2.6 Finite Element Discretization 12
2.6.1 Hexahedral Elements 13
2.6.1.1 Strain Matrix 13
2.6.1.2 Element Matrix 17
3 BACKGROUND ON SOIL BEHAVIOR UNDER MONOTONIC LOADING 19
3.1 Duncan & Chang Model 20
3.2 Determination of Experimental Values and Parameters 23
3.2.1 Initial Tangent Modulus 23
3.2.2 Modulus Constants 23
3.2.3 Cohesion and Friction Angle 24
3.2.4 Failure Ratio 25
3.2.5 Modulus Number for Unloading and Reloading 26
3.3 Modifications of Duncan & Chang 27
4 BACKGROUND ON SOIL BEHAVIOR UNDER CYCLIC LOADING . . 31
4.1 Soil Response to Cyclic Loading 32
4.1.1 Loading Types & Frequency 32
4.1.2 Varying Load Amplitude 33
4.1.2.1 Time-Hardening Method 34
4.1.2.2 Strain-Hardening Method 34
4.1.3 Other Conditions Affecting Permanent Strain 35
4.2 Behavior Types of Cyclic Loaded Soil 36
4.2.1 Plastic Shakedown 36

4.2.2 Incremental Collapse 37
4.2.3 Plastic Creep 37
4.3 Prediction of Permanent Deformation 37
4.3.1 Explicit Method 38
4.3.1.1 Plastic Deformation vs. Number of Cycle 39
4.3.1.2 Log-Log Approach 40
5 EXPLICIT CYCLIC DUNCAN CHANG MODEL 43
5.1 Representation of ECDC 43
5.1.1 Monotonic Loading - First Cycle 44
5.1.2 Explicit Step - Rest of the Cyclic Loading 45
5.1.3 Reloading 46
5.2 Determination of Explicit Parameters 47
5.2.1 Determination of Intercept Coefficient 48
5.2.2 Determination of Slope Coefficient 49
5.3 ANSYS - Usermat Implementation 52
5.3.1 Verification of Linear Elasticity Algorithm in D&C 55
5.3.2 Verification of the Nonlinear Algorithm in D&C 56
5.4 Analysis of A Cyclic Horizontally Loaded Monopile 59
5.4.1 Verification of Constant Load Amplitude 60
5.4.2 Verification of Varying Load Amplitude 63
6 CONCLUSIONS 67
6.1 Concluding Remarks 67
6.2 Future Perspectives 68

REFERENCES 69

LIST OF TABLES

TABLES

Table 3.1 Comparison of D&C versions 28

Table 5.1 D&C parameter of Berlin sand 47

Table 5.2 Cyclic triaxial test results 51

Table 5.3 Loose and dense sand parameters (Duncan & Chang 1970) 57

LIST OF FIGURES

FIGURES

Figure 1.1 Stress cycles and permanent strain relation 1

Figure 2.1 Domain and surface in three-dimensions 11

Figure 2.2 Hexahedral element with isoparametric mapping 13

Figure 3.1 Nonlinearity of stress-strain relation 19

Figure 3.2 Determination of E_i in D&C 23

Figure 3.3 Mohr–Coulomb failure envelope 25

Figure 3.4 Mohr–Coulomb failure criterion in principal stress space 25

Figure 3.5 Determination of unloading & reloading modulus 26

Figure 3.6 Flow chart of D&C 27

Figure 4.1 Monopile and foundation subjected to cyclic loading 31

Figure 4.2 Loading types 33

Figure 4.3 Comparison of methods to estimate effects of varying load amplitude 34

Figure 4.4 Behavior types of cyclic loaded soil 36

Figure 4.5 Cumulative plastic strain vs. number of load cycles 41

Figure 4.6 Log-log scaled cumulative plastic strain vs. number of load cycles 41

Figure 5.1 Stress-strain curve of monotonic and cyclic loading process . . . 44

Figure 5.2 Monotonic loading stage . . . 45

Figure 5.3 Cyclic loading stage . . . 45

Figure 5.4 Details of all loading steps . . . 46

Figure 5.5 Cyclic triaxial test results with different Δq . . . 48

Figure 5.6 Cyclic triaxial test scheme . . . 48

Figure 5.7 First cycle of $\Delta q = 237\ kPa$ . . . 49

Figure 5.8 Displacement at the end of the first cycle, $\Delta q = 237\ kPa$ . . . 50

Figure 5.9 Displacement at the end of the first cycle, $\Delta q = 153\ kPa$ . . . 50

Figure 5.10 Nonlinear regression of cyclic triaxial test data for $\Delta q = 237\ kPa$ 51

Figure 5.11 Nonlinear regression of cyclic triaxial test data for $\Delta q = 153\ kPa$ 51

Figure 5.12 ANSYS-Usermat working scheme . . . 53

Figure 5.13 Linear elastic comparison of Usermat.f vs. ANSYS built-in model for displacement in the z-direction . . . 55

Figure 5.14 Modeling triaxial test . . . 58

Figure 5.15 ANSYS Usermat.f simulation vs. D&C (1970) triaxial test (loose sand) . . . 59

Figure 5.16 ANSYS Usermat.f simulation vs. D&C (1970) triaxial test (dense sand) . . . 60

Figure 5.17 Dimension of monopile & loading scheme . . . 61

Figure 5.18 Test details of Tasan [43] . . . 62

Figure 5.19 3D meshed model of design . . . 63

Figure 5.20 x-direction displacement after 15000 cycles . . . 64

Figure 5.21 Monopile under constant amplitude load 65

Figure 5.22 Monopile under varying amplitude load 66

LIST OF ABBREVIATIONS

ABBREVIATIONS

2D	2 Dimensional
3D	3 Dimensional
D&C	Duncan & Chang material model (1970)
FEM	Finite element method
DEM	Discrete element method
UGM	Unbound granular materials
e.g.	For example
ECDC	Explicit Cyclic Duncan Chang model

CHAPTER 1

INTRODUCTION

Granular materials is a term that embodies soil, concrete, rock, and asphalt type of materials that have voids and fractures substituted with fluids in their granular skeletons [1]. They exhibit complex behavior under stress since their multiphase nature distributes it to all parts. Another essential feature of granular materials is that confining pressure has a drastic impact on their behavior and strength. Dilatancy, volume change under shear stress, is another characteristic property of them. Furthermore, granular materials have a critical state in which soil flows as a frictional fluid when it is distorted up to their ultimate condition, and it is independent of the initial state of the material [2]. Lastly, granular materials demonstrate increasing permanent strain when subjected to repeated stress cycles with equal or varying amplitudes.

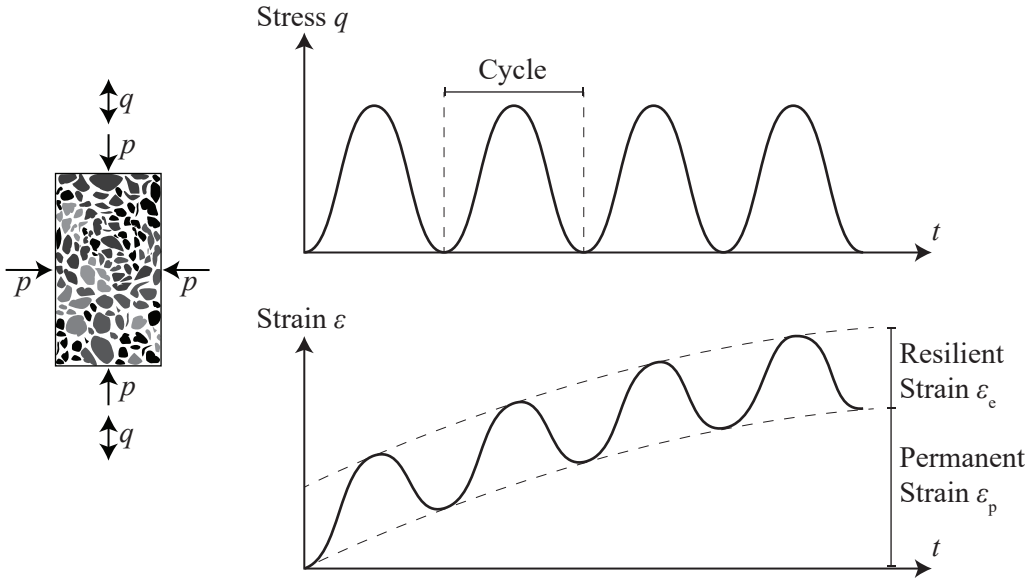

Figure 1.1: Stress cycles and permanent strain relation

This study focuses on one of the aforementioned features of granular materials that is strain response to cyclic loading, illustrated in Figure 1.1. If a soil is exposed to cyclic loading, permanent strain occurs, irrespective of whether the applied stress is greater or lower than the plastic yield strength. This behavior contradicts elastic theory. There is a proportional relation between permanent strain and the number of load cycles applied. Cumulative permanent strain, which brings about residual settlement, increases with the number of loading cycles.

1.1 Problem Definition and Motivation

Permanent deformation in granular materials leads to a wide variety of challenges in civil engineering structures such as highway pavements, railway structures, foundations of offshore and onshore wind turbines, marine structures, hydrostatically loaded silos, hydraulic structures, machine foundations, and various other cyclically loaded structures. The adverse effect of undesirable permanent deformation is the diminished structural performance. For example, pavement rutting, which is residual settlement caused by cyclic loading by vehicles, is one of the prominent failure concerns of highways. Furthermore, differential settlement may occur in a structure near a railway due to repeated loading [3]. As another example, the head shift of monopiles may take place due to cyclic loading by wind and waves. However, the prediction of deformation with experimental testing is costly and time-consuming due to the high number of load cycles required.

Numerical prediction of permanent settlement due to cyclic loading is essential for related structures in order to take certain design measures. However, it is challenging for several reasons. Firstly, the behavior of granular materials subjected to both monotonic and cyclic loading is nonlinear and intricate. It depends not only on external factors but also on numerous internal parameters. The literature provides plenty of different material models to define the behavior of granular materials. Secondly, there are multiple scale approaches (micro, meso, macro) for geomaterials because of their multiphase nature. Each scale requires a distinct understanding and tools to constitute a model. For example, in this thesis, soil behavior is investigated at the macroscopic scale, as a continuum body. Hence the finite element method (FEM)

is utilized. Thirdly, certain structures (e.g., off-shore wind turbines) are subjected to a high number (over 10^5) of repeated loading cycles. These structures need a tremendous amount of computational resources to be implicitly analyzed due to their sophisticated design. Moreover, every finite element solution produces an error as a by-product. For instance, implicit FEM analysis of a monopile loaded with 10^5 cycles magnifies the error 10^5 times which can lead to serious deviation. Fourthly, structures subjected to cyclic loading have complex geometries which demand three-dimensional (3D) analysis. Lastly, soil-structure interaction influences stress distribution in soil and the friction created by this interaction has an impact on the deformation. As a consequence of these, the behavior of granular materials exposed to cyclic loading is complex, and the prediction of permanent deformation is an involved task.

1.2 Outline of Thesis

This thesis concentrates on the challenging subject of developing a practical 3D method capable of modeling granular materials subjected to both monotonic and cyclic loading. Chapter 2 provides background knowledge on computational modeling of granular materials. Chapters 3 and 4 provide information on methods investigated, Chapter 5 presents a new model with an example, and finally, Chapter 6 concludes the thesis. More specifically:

- Chapter 2 introduces a background of computational methods detailed in the following chapters. A brief timeline of geomechanics constitutive modeling is introduced. A variety of equations are specified to solve an initial boundary value problem of soil as a 3D continuum body. Conservation laws are also mentioned. Next, a constitutive equation is discussed. The weak form is constructed based on the strong form. Approximations required to fulfill weak formulation are stated. Details of the hexahedral element i.e. shape functions, strain, and element matrices, are elaborated.

- Chapter 3 provides a detailed explanation of the Duncan & Chang model (D&C), which is a nonlinear elastic constitutive relation for granular materials. To understand their behavior under cyclic loading, the behavior of granular materials

under monotonic loading needs to be investigated. In view of this, Chapter 3 explores the monotonic loading and unloading behavior of soil by D&C. Moreover, nonlinearity of the stress-strain curve is explained. The experimental and numerical processes of determining parameters of D&C are mentioned. Then, the assessment of loading, unloading, reloading conditions and mathematical background of tangent moduli in D&C are explained step by step. Modifications to D&C proposed since 1970 are shown.

- Chapter 4 presents an overall perspective on the behavior of granular materials subjected to cyclic loading. It begins by defining permanent deformation under cyclic loading and how soil reacts to cyclic loading. Then, loading types and frequency are detailed. The time-hardening and strain-hardening methods are explained in order to understand the behavior of soil under varying load amplitude. Effects of permeability, relative density, moisture content, density, stress history, grading, and aggregate size are mentioned. Behavior types of cyclically loaded soil, namely plastic shakedown, plastic creep, and incremental collapse, are mentioned. A summary of the literature on prediction methods of permanent deformation is presented. Explicit methods based on number of cycles are compared. The log-log approach is further specified.

- Chapter 5 introduces the Explicit Cyclic Duncan Chang (ECDC) model that combines the Duncan & Chang model with the explicit permanent deformation approach. Firstly, the fundamental representation of ECDC is provided. After that, it is thoroughly investigated in monotonic loading, cyclic loading and reloading. The rheological device of ECDC is illustrated. Then, the determination of the necessary cyclic parameters is detailed. The implementation of ECDC into the finite element solver is elaborated. The ECDC algorithm scheme is provided. The verification of the D&C algorithm is performed using two different relative density sands. Finally, to examine the performance of ECDC, a 3D horizontally cyclic loaded monopile, anchored in sand is analyzed with the ECDC model. The first analysis is conducted with constant load amplitude whereas the second is conducted with varying load amplitude.

- Chapter 6 highlights the concluding remarks and contributions and provides future perspectives.

CHAPTER 2

A SURVEY OF COMPUTATIONAL MODELING OF GRANULAR MATERIALS

In this chapter, background information and basic concepts that will be needed for modeling are given. Firstly, a timeline of the constitutive modeling of geomechanics is introduced. Furthermore, the fundamental principles related to the computational tools utilized in this study are detailed. Soil is modeled as a continuum body, and therefore, it is solved as a boundary value problem using finite element principles. Details of linear isotropic elasticity of a 3D element are elaborated. The strain and the element matrices are illustrated.

2.1 Brief Timeline of Granular Materials Constitutive Modeling

The timeline of constitutive modeling starts in 1678, with Hooke's law of linear elasticity. In 1773, the Coulomb failure criterion, which is the earliest work on plasticity, was stated. The failure criterion and plasticity were further developed by Tresca [4], von Mises [5], and Drucker [6]. However, those yield criteria don't work for granular materials since their dependence on confining pressure isn't considered. In 1952, a hydrostatic pressure dependent yield criterion was offered by Drucker and Prager [7]. In the 1960s, the critical state condition was proposed by researchers at Cambridge University [8, 9, 2]. Moreover, models based on the incremental nonlinearity of soil under monotonic loading have been proposed in the literature. One example of such a model is Duncan & Chang [10] and another constitutive model is hypoplasticity with many more parameters involved [11].

Laboratory tests are essential to determine the intricate behavior of granular materials.

In this regard, one of the first laboratory tests was conducted in 1943. Buchanan and Kuri performed the first cyclic triaxial test in 1956 [1]. One of the substantial findings of repeated loading test is that even if two separate soil samples exhibit similar behavior under monotonic loading, their cyclic loading response can be distinct [12]. Furthermore, finding of these tests advances earthquake studies and the liquefaction phenomenon of cohesionless granular materials [13, 14].

In the 1970s, with the momentum of the oil industry, construction of off-shore petroleum structures proliferated. These structures, which are subjected to repeated loading of winds, waves, and currents, drew attention to the performance of granular materials. Moreover, studies on pavement and traffic loading also became widespread in this era.

In the early 1980s, constitutive modeling of soil under cyclic loading did not exist despite the advancement in modeling of soil subjected to monotonic loading [1]. Thus, the relationship between the number of load cycles and permanent deformation in granular materials was determined by analytical methods.

In past decades, behavior of granular materials induced by cyclic loading has been examined by both analytical methods based on laboratory tests, and constitutive relations built upon plasticity and viscosity theories, and shakedown theory [15, 16, 17, 3, 18, 19, 20]. Other than the above-mentioned models, densification, kinematic hardening, bounding surface, generalized plasticity model, and multi-laminate models have been proposed to describe different soil behavior under various external conditions [21].

2.2 Application of the Finite Element Method in Granular Materials

There are two common approaches to solving a boundary value problem of granular materials, namely the finite element method and the discrete element method (DEM). Even though it is more appropriate to treat granular materials as a discrete form, DEM is not an efficient approach to handle large boundary value problems due to its computational cost [22].

In general, to solve an initial boundary value problem using the finite element method, four types of equations are required:

- Laws of conservation (Balance equations)
- Constitutive equations (Material laws)
- Boundary conditions
- Initial conditions

The details of these equations are mentioned in the following sections.

2.3 Laws of Conservation

The behavior of a continuum body of granular materials subjected to monotonic and cyclic loading follow laws of solid mechanics elasticity problems under small deformation. Strong form of equation (partial differential equation) is instituted based on conservation of linear momentum

$$\int \rho b dV + \int \text{div}(\sigma) dV = \frac{d}{dt} \int \rho v dV \tag{2.1}$$

where σ is the Cauchy stress, b is the body force vector, ρ is the density function, and v is the velocity vector. As the problem studied in this thesis is quasi-static, balance equation of linear momentum can be written as

$$\text{div}(\sigma) + \rho b \equiv (\sigma_{ji,j} + \rho b_i) i_i = 0 \tag{2.2}$$

where i is the free index and j is the dummy index [23]. The Cauchy stress tensor, $\sigma_{ji,j}$, can be represented as summation takes place over repeated indices:

$$\sigma_{ji,j} \equiv \sum_{j=1}^{3} \sigma_{ji,j} = \sigma_{1i,1} + \sigma_{2i,2} + \sigma_{3i,3} \tag{2.3}$$

2.3.1 Internal Energy in Solids

Assume that a major axial stress σ_1, which is one of the three direct stress components, is acting on both opposite surfaces of an infinitesimal solid element. As a result, displacements of u_1 and $u_1 + du_1$ are produced at x_1 and $x_1 + dx_1$. Axial strain becomes $\varepsilon_1 = \partial u_1/\partial x_1$ and the force acting on the surface can be written as $\sigma_1 dx_2 dx_3$ [24]. Total internal work of axial stress on the whole volume, V, of body B, can be found by integration as follows

$$W_I = -\int \sigma_1 dx_2 dx_3 du_1 = -\int_B \sigma_1 \frac{du_1}{dx_1} dx_1 dx_2 dx_3 = -\int_B \sigma_1 \varepsilon_1 dV \tag{2.4}$$

in which W_I is the work done by internal stress. Considering contributions from all stress components and inserting the stress definition in Equation 2.3, internal energy can be expressed as

$$W = \sigma_{ij}\varepsilon_{ij} \tag{2.5}$$

where indices indicate double summation, so:

$$\begin{aligned} W = \quad & \sigma_{11}\varepsilon_{11} + \sigma_{12}\varepsilon_{12} + \sigma_{13}\varepsilon_{13} \\ & + \sigma_{21}\varepsilon_{21} + \sigma_{22}\varepsilon_{22} + \sigma_{23}\varepsilon_{23} \\ & + \sigma_{31}\varepsilon_{31} + \sigma_{32}\varepsilon_{32} + \sigma_{33}\varepsilon_{33} \end{aligned} \tag{2.6}$$

Finally, those nine terms can be represented with six terms due to symmetry (from conservation of angular momentum):

$$W = \sigma_{11}\varepsilon_{11} + \sigma_{22}\varepsilon_{22} + \sigma_{33}\varepsilon_{33} + 2(\sigma_{12}\varepsilon_{12} + \sigma_{23}\varepsilon_{23} + \sigma_{31}\varepsilon_{31}) \tag{2.7}$$

The reduction in the number of terms alleviates the memory resource requirements and speeds up the calculation process. This reduced order of the matrix is called the Voigt notation [25].

2.4 Material Equation

The behavior of a granular material under monotonic loading is nonlinear. The Duncan & Chang model (D&C) is utilized as the material equation for monotonic loading stage in this thesis. D&C uses a pressure dependent elastic modulus to achieve nonlinearity of granular materials. For every load increment, it determines a new tangent modulus, updates the stiffness matrix and solves the sub-step linear elastically. It reiterates this process for each load sub-step. The constitutive model is tweaked based on isotropic generalized Hooke's formulation. Thus, material equation is detailed based on isotropic linear elasticity.

Consider the isotropic linear elastic material model; then, free energy can be represented as [26, 27, 23]

$$\psi(\varepsilon) = \frac{1}{2}\varepsilon_{ij} C_{ijkl} \varepsilon_{kl} \tag{2.8}$$

where C is 4^{th} order stiffness matrix with the form of $C = C_{ijkl} i_i \otimes i_j \otimes i_k \otimes i_l$, $\psi(\varepsilon)$ is the free energy function based on strain. The derivative of free energy formulation provides:

$$\sigma_{ij} = \frac{\partial \psi}{\partial \varepsilon_{ij}} = C_{ijkl} \varepsilon_{kl} \tag{2.9}$$

For efficiency increases on memory space, Equation 2.9 can be expressed in matrix form

$$[\sigma] = [C] : [\varepsilon] \tag{2.10}$$

where $[\sigma]$ is the 2^{nd} order stress tensor, $[\varepsilon]$ is 2^{nd} order strain tensor. Element-wise

demonstration of Voigt notation matrix form can be presented as:

$$\begin{bmatrix} \sigma_{11} \\ \sigma_{22} \\ \sigma_{33} \\ \sigma_{12} \\ \sigma_{23} \\ \sigma_{31} \end{bmatrix} = \begin{bmatrix} C_{1111} & C_{1122} & C_{1133} & C_{1112} & C_{1123} & C_{1113} \\ C_{2211} & C_{2222} & C_{2233} & C_{2212} & C_{2223} & C_{2213} \\ C_{3311} & C_{3322} & C_{3333} & C_{3312} & C_{3323} & C_{3313} \\ C_{1211} & C_{1222} & C_{1233} & C_{1212} & C_{1223} & C_{1213} \\ C_{2311} & C_{2322} & C_{2333} & C_{2312} & C_{2323} & C_{2313} \\ C_{1311} & C_{1322} & C_{1333} & C_{1312} & C_{1323} & C_{1313} \end{bmatrix} : \begin{bmatrix} \varepsilon_{11} \\ \varepsilon_{22} \\ \varepsilon_{33} \\ 2\varepsilon_{12} \\ 2\varepsilon_{23} \\ 2\varepsilon_{31} \end{bmatrix} \tag{2.11}$$

Furthermore, C_{ijkl} can be written in indicial form with Lamé constants (λ, μ), as

$$C_{ijkl} = \lambda\delta_{ij}\delta_{kl} + \mu(\delta_{ik}\delta_{jl} + \delta_{il}\delta_{jk}) = \lambda\mathbf{1} \otimes \mathbf{1} + 2\mu[] \tag{2.12}$$

$$\lambda = \frac{E \cdot \nu}{(1+\nu)(1-2\nu)} \tag{2.13}$$

$$\mu = \frac{E}{2(1+\nu)} \tag{2.14}$$

where $\mathbf{1}$ is $[1,1,1,0,0,0]^T$, **[]** is the 4^{th} order identity tensor, δ_{ij} is the Kronecker delta, E is the elastic modulus, and ν is Poisson's ratio. The matrix form of C with Lamé constants then becomes:

$$C = \begin{bmatrix} \lambda+2\mu & \lambda & \lambda & 0 & 0 & 0 \\ \lambda & \lambda+2\mu & \lambda & 0 & 0 & 0 \\ \lambda & \lambda & \lambda+2\mu & 0 & 0 & 0 \\ 0 & 0 & 0 & \mu & 0 & 0 \\ 0 & 0 & 0 & 0 & \mu & 0 \\ 0 & 0 & 0 & 0 & 0 & \mu \end{bmatrix} \tag{2.15}$$

Overall, the matrix form of $\sigma = C : \varepsilon$ is shown below:

$$\begin{bmatrix} \sigma_{11} \\ \sigma_{22} \\ \sigma_{33} \\ \sigma_{12} \\ \sigma_{23} \\ \sigma_{31} \end{bmatrix} = \begin{bmatrix} \lambda+2\mu & \lambda & \lambda & 0 & 0 & 0 \\ \lambda & \lambda+2\mu & \lambda & 0 & 0 & 0 \\ \lambda & \lambda & \lambda+2\mu & 0 & 0 & 0 \\ 0 & 0 & 0 & \mu & 0 & 0 \\ 0 & 0 & 0 & 0 & \mu & 0 \\ 0 & 0 & 0 & 0 & 0 & \mu \end{bmatrix} : \begin{bmatrix} \varepsilon_{11} \\ \varepsilon_{22} \\ \varepsilon_{33} \\ 2\varepsilon_{12} \\ 2\varepsilon_{23} \\ 2\varepsilon_{31} \end{bmatrix} \tag{2.16}$$

2.5 Weak Form

Before starting with details of weak form, it should be stated there are minor differences between two-dimensional and three-dimensional finite element analysis, mainly in the terms and definitions of mathematical expressions and vector notation [28]. On the other hand, the structure of weak and strong formulations are typical. At first, unit vectors of $\vec{i}$, $\vec{j}$, $\vec{k}$ are employed to define vector $\vec{t}\,(= q_x\vec{i} + q_y\vec{j} + q_z\vec{k})$ on surface ∂B of the three-dimensional domain B which are illustrated in Figure 2.1. In continuum mechanics, stress traction ($\vec{t}$) is a fundamental quantity defined by the unit surface normal ($\vec{n}$). The relationship between these variable is established by Cauchy's theorem as $\vec{t} = \vec{\sigma}\vec{n}$.

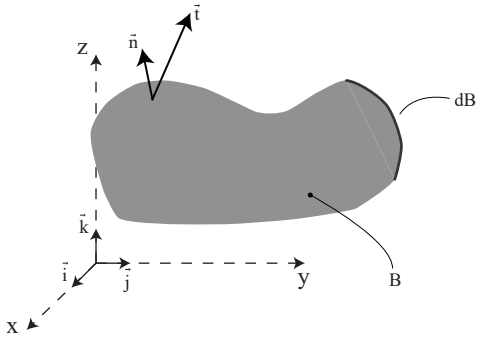

Figure 2.1: Domain and surface in three-dimensions

There are two types of boundary conditions on surface ∂B which are Essential (Dirichlet, displacement $u = \bar{u}$ on ∂B_u) boundaries and Natural (Neumann, traction $t = \bar{t}$ on ∂B_t) boundaries. Moreover, finite element discretization divides body B into sub-

domains of B_e while it splits up boundary (surface for 3D geometry) into subsurfaces of ∂B_e [29, 26].

After defining boundary conditions and other terms, weak form can be approximated through Galerkin formulation by multiplying strong form (2.2) with variational function of $\delta u(x,t)$ as follows:

$$\begin{aligned}\delta\hat{\Pi}_{eq} = &\sum_e \left[\int_{B_e} \delta(\mathcal{S}\mathbf{u})^T \sigma \, \mathrm{d}V - \int_{B_e} \delta\mathbf{u}^T \mathbf{b} \, \mathrm{d}V\right] \\ &- \sum_{et} \left[\int_{\partial B_{te}} \delta\mathbf{u}^T \mathbf{t} \, \mathrm{d}A\right] = 0\end{aligned} \tag{2.17}$$

This virtual form requires approximations of u and δu.

2.6 Finite Element Discretization

To fulfill weak formulation, approximation of u and δu must be assumed. In element domain, displacement $u(x,t)$ can be derived as

$$u(x,t) \approx N(x)d^e \tag{2.18}$$

where $N(x)$ is the shape function matrix, d^e is the nodal displacement vector. Furthermore, the strain field $\varepsilon(x,t)$ is described by

$$\varepsilon(x,t) = \mathcal{S}u \approx B(x)d^e \tag{2.19}$$

where $B(x)$ is the strain matrix. Virtual displacement $\delta u(x,t)$ is approximated as

$$\delta u(x,t) \approx N(x)\delta d^e \tag{2.20}$$

and further, virtual strain $\delta\varepsilon$ can be computed by

$$\delta\varepsilon = B\delta d^e \tag{2.21}$$

in which δd^e is called the virtual nodal displacement vector or the nodal variation vector. To establish shape function $N(x)$ and strain matrix $B(x)$, the element type that will mesh the body has to be determined. For comprehensive 3D analysis, the 3D hexahedral solid element type is selected.

2.6.1 Hexahedral Elements

There are two fundamental three-dimensional solid finite element types, which are tetrahedral and hexahedral [28]. The Tetrahedral element corresponds to the triangular element in 2D, whereas hexahedral is the equivalent of the quadrilateral element in 2D. All element types have higher and lower-order elements. In this study, we will focus on the lower order, 8-node hexahedral element.

2.6.1.1 Strain Matrix

Hexahedral is the element with the shape of hexahedron, which has eight nodes and six surfaces, illustrated in Figure 2.2 [30].

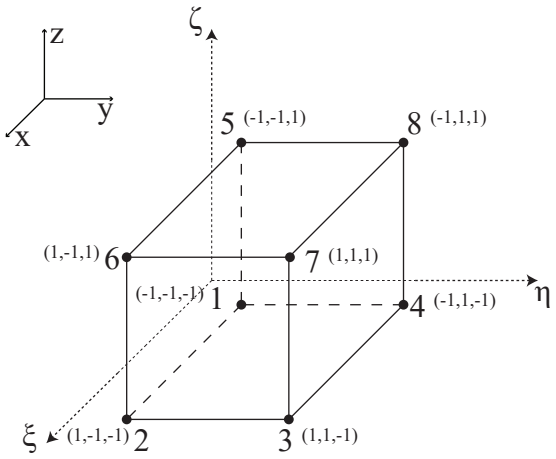

Figure 2.2: Hexahedral element with isoparametric mapping

It has the origin at the center of the hexahedron with an isoparametric natural coordinate system (ξ, η, ζ). Shape functions with natural coordinate system curate the

relation between global and local coordinate systems as [26, 31, 32]

$$\begin{Bmatrix} x \\ y \\ z \end{Bmatrix} = \sum_{i=1}^{8} \left(\begin{bmatrix} N_i & 0 & 0 \\ 0 & N_i & 0 \\ 0 & 0 & N_i \end{bmatrix} \begin{Bmatrix} x_i \\ y_i \\ z_i \end{Bmatrix} \right) \tag{2.22}$$

where the trilinear shape function N is expressed by

$$N_i = \frac{1}{8}(1 + \xi\xi_i)(1 + \eta\eta_i)(1 + \zeta\zeta_i) \tag{2.23}$$

in which ξ_i, η_i, ζ_i correspond to node i of the natural coordinates [30]. Shape functions of the eight nodes can be then written as:

$$\begin{aligned} N_1 &= \frac{1}{8}(1 - \xi)(1 - \eta)(1 - \zeta) \\ N_2 &= \frac{1}{8}(1 + \xi)(1 - \eta)(1 - \zeta) \\ N_3 &= \frac{1}{8}(1 + \xi)(1 + \eta)(1 - \zeta) \\ N_4 &= \frac{1}{8}(1 - \xi)(1 + \eta)(1 - \zeta) \\ N_5 &= \frac{1}{8}(1 - \xi)(1 - \eta)(1 + \zeta) \\ N_6 &= \frac{1}{8}(1 + \xi)(1 - \eta)(1 + \zeta) \\ N_7 &= \frac{1}{8}(1 + \xi)(1 + \eta)(1 + \zeta) \\ N_8 &= \frac{1}{8}(1 - \xi)(1 + \eta)(1 + \zeta) \end{aligned} \tag{2.24}$$

Moreover, the nodal displacement vector can be stated as

$$d^e = \begin{bmatrix} d_1^e \\ d_2^e \\ d_3^e \\ d_4^e \\ d_5^e \\ d_6^e \\ d_7^e \\ d_8^e \end{bmatrix}_{24x1} \tag{2.25}$$

where the displacement component of each node is

$$d_i^e = \begin{bmatrix} u_1 \\ v_2 \\ w_3 \end{bmatrix} \text{ for i = 1,2,3,4,5,6,7,8} \tag{2.26}$$

The shape function matrix is constructed with eight sub-matrices of N_i:

$$N = \begin{bmatrix} N_1 & 0 & 0 & ... & N_8 & 0 & 0 \\ 0 & N_1 & 0 & ... & 0 & N_8 & 0 \\ 0 & 0 & N_1 & ... & 0 & 0 & N_8 \end{bmatrix}_{3x24} \tag{2.27}$$

Furthermore, to compute $[\varepsilon] = Bd^e$, the strain interpolation matrix (B-matrix), B, need to be extracted. Regarding this, the strain matrix can be defined as

$$B = \begin{bmatrix} B_1 & B_2 & B_3 & B_4 & B_5 & B_6 & B_7 & B_8 \end{bmatrix}_{6x24} \tag{2.28}$$

in which

$$B_i = \begin{bmatrix} \partial N_i/\partial x & 0 & 0 \\ 0 & \partial N_i/\partial y & 0 \\ 0 & 0 & \partial N_i/\partial z \\ 0 & \partial N_i/\partial z & \partial N_i/\partial y \\ \partial N_i/\partial z & 0 & \partial N_i/\partial x \\ \partial N_i/\partial y & \partial N_i/\partial x & 0 \end{bmatrix} \text{ for i = 1,2,3,4,5,6,7,8} \tag{2.29}$$

To acquire $\partial N_i/\partial x,\ \partial N_i/\partial y,\ \partial N_i/\partial z$ in B matrix, chain rule for partial derivative is utilized.

$$\begin{Bmatrix} \partial N_i/\partial \xi \\ \partial N_i/\partial \eta \\ \partial N_i/\partial \zeta \end{Bmatrix} = \begin{bmatrix} \partial x/\partial \xi & \partial y/\partial \xi & \partial z/\partial \xi \\ \partial x/\partial \eta & \partial y/\partial \eta & \partial z/\partial \eta \\ \partial x/\partial \zeta & \partial y/\partial \zeta & \partial z/\partial \zeta \end{bmatrix} \begin{Bmatrix} \partial N_i/\partial x \\ \partial N_i/\partial y \\ \partial N_i/\partial z \end{Bmatrix} \tag{2.30}$$

$$J = \begin{bmatrix} \partial x/\partial \xi & \partial y/\partial \xi & \partial z/\partial \xi \\ \partial x/\partial \eta & \partial y/\partial \eta & \partial z/\partial \eta \\ \partial x/\partial \zeta & \partial y/\partial \zeta & \partial z/\partial \zeta \end{bmatrix} \tag{2.31}$$

where [J] is Jacobian and it can be written by substituting Equation 2.22 into Equation 2.31:

$$J = \begin{bmatrix} \frac{\partial N_1}{\partial \xi} & \frac{\partial N_2}{\partial \xi} & \frac{\partial N_3}{\partial \xi} & \frac{\partial N_4}{\partial \xi} & \frac{\partial N_5}{\partial \xi} & \frac{\partial N_6}{\partial \xi} & \frac{\partial N_7}{\partial \xi} & \frac{\partial N_8}{\partial \xi} \\ \frac{\partial N_1}{\partial \eta} & \frac{\partial N_2}{\partial \eta} & \frac{\partial N_3}{\partial \eta} & \frac{\partial N_4}{\partial \eta} & \frac{\partial N_5}{\partial \eta} & \frac{\partial N_6}{\partial \eta} & \frac{\partial N_7}{\partial \eta} & \frac{\partial N_8}{\partial \eta} \\ \frac{\partial N_1}{\partial \zeta} & \frac{\partial N_2}{\partial \zeta} & \frac{\partial N_3}{\partial \zeta} & \frac{\partial N_4}{\partial \zeta} & \frac{\partial N_5}{\partial \zeta} & \frac{\partial N_6}{\partial \zeta} & \frac{\partial N_7}{\partial \zeta} & \frac{\partial N_8}{\partial \zeta} \end{bmatrix} \begin{bmatrix} x_1 & y_1 & z_1 \\ x_2 & y_2 & z_2 \\ x_3 & y_3 & z_3 \\ x_4 & y_4 & z_4 \\ x_5 & y_5 & z_5 \\ x_6 & y_6 & z_6 \\ x_7 & y_7 & z_7 \\ x_8 & y_8 & z_8 \end{bmatrix} \tag{2.32}$$

Lastly, multiplying Equation 2.30 with the inverse of [J] provides required parameters

in the strain matrix.

$$\begin{Bmatrix} \partial N_i/\partial x \\ \partial N_i/\partial y \\ \partial N_i/\partial z \end{Bmatrix} = J^{-1} \begin{Bmatrix} \partial N_i/\partial \xi \\ \partial N_i/\partial \eta \\ \partial N_i/\partial \zeta \end{Bmatrix} \tag{2.33}$$

2.6.1.2 Element Matrix

For a single element, Equations 2.18, 2.19, 2.20, 2.21 can be inserted into Galerkin Equation 2.17 as

$$\delta\hat{\Pi}^e_{eq} = \delta\mathbf{u}^T \left[\int_{B_e} \mathbf{B}^T\boldsymbol{\sigma}\ \mathrm{d}V\right] - \delta\mathbf{u}^T \left[\int_{B_e} \mathbf{N}^T\mathbf{b}\ \mathrm{d}V + \int_{\partial B_{t_e}} \mathbf{N}^T\mathbf{t}\ \mathrm{d}A\right] \tag{2.34}$$

where

$$f^e_{int} = \int_{B^e} B^T[\sigma]\ \mathrm{d}V \tag{2.35}$$

$$f^e_{ext} = \int_{B^e} N^T b\ \mathrm{d}V + \int_{B^e} N^T t\ \mathrm{d}A \tag{2.36}$$

where $\int_{B^e} N^T b\ \mathrm{d}V$ provides body forces, $\int_{B^e} N^T t\ \mathrm{d}A$ gives surface (traction) forces. $\sum f^e_{int} = \sum f^e_{ext}$ equality holds for the quasi-static problem. Furthermore, substituting Equation 2.10 and 2.19 into Equation 2.35 provides:

$$k^e = \int_{B^e} B^T[C]B\ \mathrm{d}V \tag{2.37}$$

that ensures $f^e_{int} = k^e d^e$ where k^e is the element stiffness matrix.

CHAPTER 3

BACKGROUND ON SOIL BEHAVIOR UNDER MONOTONIC LOADING

In this chapter, the Duncan & Chang model (D&C), which is a model that predicts the soil behavior under monotonic loading, is introduced [10]. The D&C presents the isotropic generalized Hooke's Law relation based on pressure-dependent modulus with stress increments [33]. Thus, the nonlinearity of the stress-strain curve originates from stress-dependent modulus. D&C requires several parameters to manage the association between stress and tangent modulus. In each strain increment, soil is assumed to behave linearly with the established modulus, which is calculated by the contribution of those parameters, shown in Figure 3.1.

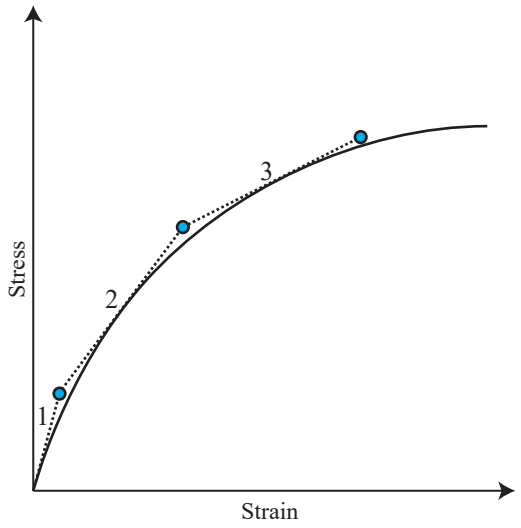

Figure 3.1: Nonlinearity of stress-strain relation

3.1 Duncan & Chang Model

Duncan & Chang [10] proposed a nonlinear material model to exhibit the hyperbolic constitutive relation of granular materials. It is a well-known nonlinear elastic model that predicts smooth stress-strain relation in soils. D&C is built upon hyperbolic constitutive equation provided by Kondner (1963)

$$\sigma_1 - \sigma_3 = \frac{\varepsilon}{a + b\varepsilon} \tag{3.1}$$

where σ_1 is the major principal stress, σ_3 is the minor principal stress, ε is the axial strain, and a, b are experimental parameters [34]. a is the reciprocal of E_i (initial tangent modulus), b is the reciprocal of $(\sigma_1 - \sigma_3)_{ult}$ (asymptotic value of stress difference):

$$a = \frac{1}{E_i} \qquad b = \frac{1}{(\sigma_1 - \sigma_3)_{ult}} \tag{3.2}$$

In general, it is known that stress difference at failure, commonly called the compressive strength, is less than the asymptotic value of stress difference and the ratio of these values represents the failure ratio R_f

$$R_f = \frac{(\sigma_1 - \sigma_3)_f}{(\sigma_1 - \sigma_3)_{ult}} \tag{3.3}$$

where $(\sigma_1 - \sigma_3)_f$ stands for stress difference at failure (compressive strength of soil). This ratio leads R_f to always be less than or equal to 1. R_f is independent of hydrostatic pressure σ_3 (also known as confining pressure). Concatenating Equation 3.2 into Equation 3.1 gives:

$$\sigma_1 - \sigma_3 = \frac{\varepsilon}{\left(\frac{1}{E_i} + \frac{\varepsilon\ R_f}{(\sigma_1 - \sigma_3)_f}\right)} \tag{3.4}$$

D&C uses a confining pressure-dependent initial tangent modulus E_i demonstrated

in experimental works by Janbu [35]

$$E_i = KP_a\left(\frac{\sigma_3}{P_a}\right)^n \tag{3.5}$$

where P_a is the atmospheric pressure with the same unit as σ_3 and E_i, K is the modulus number, and n is the exponent that represents the rate of variation of E_i. D&C utilizes Mohr–Coulomb as the failure criterion (Equation 3.6) for its stress-strain relation, and it assumes that σ_3 is constant during failure.

$$(\sigma_1 - \sigma_3)_f = \frac{2c\ cos\phi + 2\sigma_3\ sin\phi}{1 - sin\phi} \tag{3.6}$$

In equation 3.6, c is the cohesion of soil, ϕ is the friction angle. In order to form tangent modulus, which illustrates the constitutive relation, Equation 3.4 is utilized with incremental strain steps. Assumption of constant σ_3 still holds while taking the derivative of the stress function to get the tangent modulus

$$E_t = \frac{\partial(\sigma_1 - \sigma_3)}{\partial\varepsilon} \tag{3.7}$$

which becomes:

$$E_t = \frac{\frac{1}{E_i}}{\left(\frac{1}{E_i} + \frac{R_f\ \varepsilon}{(\sigma_1-\sigma_3)_f}\right)^2} \tag{3.8}$$

Reorganizing Equation 3.4 to give ε

$$\varepsilon = \frac{\sigma_1 - \sigma_3}{E_i\left(1 - \frac{R_f\ (\sigma_1-\sigma_3)}{(\sigma_1-\sigma_3)_f}\right)} \tag{3.9}$$

and substituting Equation 3.9 into Equation 3.8:

$$E_t = \left(1 - \frac{R_f\ (\sigma_1 - \sigma_3)}{(\sigma_1 - \sigma_3)_f}\right)^2 E_i \tag{3.10}$$

E_t can also be stated as

$$E_t = (1 - R_f\ S)^2 E_i \tag{3.11}$$

where S is the stress level (mobilized strength fraction):

$$S = \frac{(\sigma_1 - \sigma_3)}{(\sigma_1 - \sigma_3)_f} \tag{3.12}$$

The overall formula can then be expanded as:

$$E_t = \left(1 - \frac{R_f\ (1 - sin\phi)(\sigma_1 - \sigma_3)}{2c\ cos\phi + 2\sigma_3\ sin\phi}\right)^2 K P_a \left(\frac{\sigma_3}{P_a}\right)^n \tag{3.13}$$

In brief, the stress update process of D&C is expressed in Box 1.

Box 1: Stress update procedure used in D&C

1. Obtain stress tensor, which is in Voigt notation, and transform it into 3x3 matrix form.
2. Calculate principal stresses.
3. Compose stiffness tensor with initial tangent modulus.
4. Compute the stress level.
5. Calculate tangent modulus with stress level.
   (a) If it is unloading step, use unloading modulus.
6. Update stiffness tensor with tangent modulus.
7. Update stress tensor.

3.2 Determination of Experimental Values and Parameters

In this section, parameters in Equation 3.13 are detailed. The experimental process to obtain these parameters is also explained.

3.2.1 Initial Tangent Modulus

Initial tangent modulus E_i can be calculated as the initial tangent of the deviatoric stress vs. axial strain plot from the drained triaxial test, as shown in Figure 3.2a. E_i can also be extracted from where the plot line of the ratio of axial strain to stress difference vs. axial strain cuts the y-axis. According to Figure 3.2b, "a" can simply be determined from the graph and corresponds to $a = \frac{1}{E_i}$.

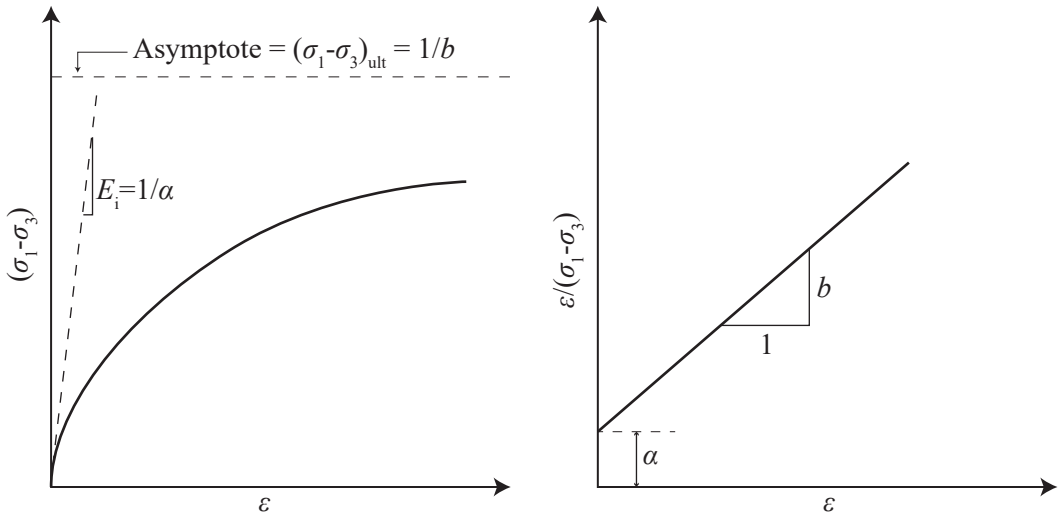

(a) Deviatoric stress vs. Axial strain

(b) Axial strain/deviatoric stress vs. Axial strain

Figure 3.2: Determination of E_i in D&C

3.2.2 Modulus Constants

Modulus constants K and n are obtained by fitting a line to the log-log plot of E_i to σ_3. Dividing both sides of Equation 3.5 by P_a generates $\frac{E_i}{P_a} = K\left(\frac{\sigma_3}{P_a}\right)^n$ equation and taking then logarithms linearizes the equation to give the parameters. Several triaxial

tests with different confining pressures are required to get a better fit. To increase the fitness of data, triaxial tests should be conducted under similar principle stresses [36].

3.2.3 Cohesion and Friction Angle

In soil mechanics, the Mohr–Coulomb yield criterion is one of the most prevalent methods to estimate plastic yield strength. The Mohr—Coulomb failure envelope relies on the linear relation between normal and shear stress as illustrated in Figure 3.3

$$\tau = c + \sigma_n \cdot tan(\phi) \tag{3.14}$$

where τ is the shear stress and σ_n is the normal stress [37]. Cohesion c represents the resistance of intermolecular bonds between the grains. Its value is taken as the y-axis intercept of the tangent to the circle with. The Friction angle ϕ describes the granular friction, which forms the shear strength of soil, also known shearing resistance [38]. It is the angle between the tangent to the circle and the x-axis. Hence, from Figure 3.3:

$$\tau = \frac{\sigma_1 - \sigma_3}{2} \cdot cos(\phi) \tag{3.15}$$

$$\sigma_n = \frac{\sigma_1 + \sigma_3}{2} + \frac{\sigma_1 - \sigma_3}{2} \cdot sin(\phi) \tag{3.16}$$

Substituting Equation 3.15 and 3.16 into 3.14 yields

$$\sigma_1 - \sigma_3 + (\sigma_1 + \sigma_3) \cdot sin(\phi) = 2c \cdot cos(\phi) \tag{3.17}$$

Using equation 3.17 as yield function and replacing $(\sigma_1 - \sigma_3)$ with $(\sigma_1 - \sigma_3)_f$, then rewriting σ_1 in terms of σ_3 produces Equation 3.6 which retains the assumption that confining pressure σ_3 is constant during the failure [10]. Figure 3.4 describes the Mohr–Coulomb yield criterion in principal stress space. It should be mentioned that

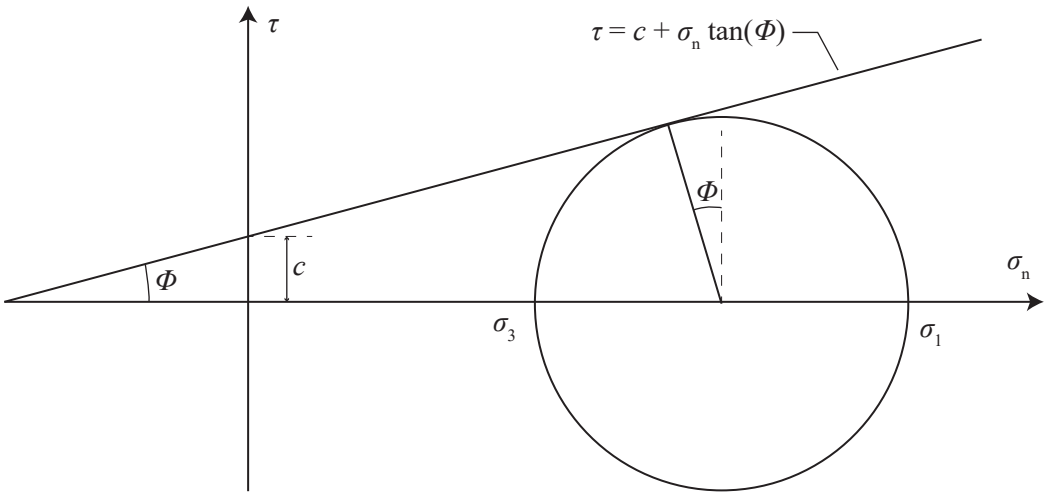

Figure 3.3: Mohr–Coulomb failure envelope

D&C is insensitive to variation in intermediate principal stress (σ_2) so that stress in or on the yield surface is always symmetrical to σ_2 and σ_3 axes.

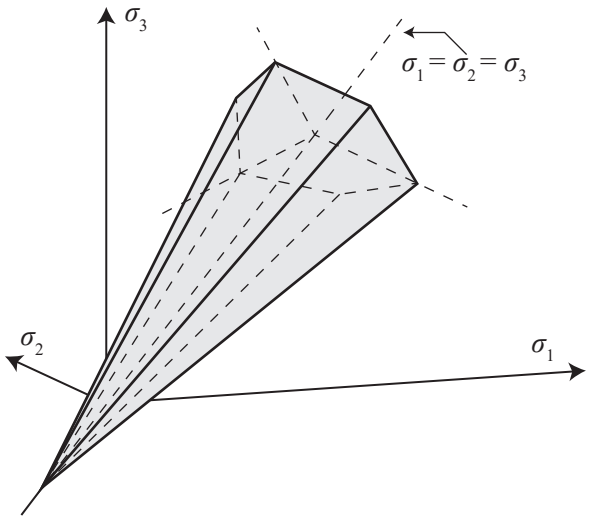

Figure 3.4: Mohr–Coulomb failure criterion in principal stress space

3.2.4 Failure Ratio

Deviatoric stress at failure $(\sigma_1 - \sigma_3)_f$ is computed with Mohr–Coulomb's failure criterion which requires c, ϕ and confining pressure σ_3 (Equation 3.6). Next, asymptotic value at deviatoric stress $(\sigma_1 - \sigma_3)_{ult}$ should be estimated from the $\frac{\varepsilon}{\sigma_1 - \sigma_3}$ vs. ε plot

(Figure 3.2b). The slope of this graph delivers reciprocal of $(\sigma_1 - \sigma_3)_{ult}$. Finally, failure ratio R_f is calculated by dividing $(\sigma_1 - \sigma_3)_f$ to $(\sigma_1 - \sigma_3)_{ult}$.

3.2.5 Modulus Number for Unloading and Reloading

It has been shown that the unloading and reloading moduli are equal and independent of the stress level and strain of the soil. As illustrated in Figure 3.5, the constitutive relation of soil during unloading and reloading is considered linear and elastic [10]. The unloading and reloading modulus can be formulated as

$$E_{ur} = K_{ur} P_a \left(\frac{\sigma_3}{P_a}\right)^n \tag{3.18}$$

where E_{ur} is the unloading and reloading modulus, K_{ur} is the modulus number. n is the same as in Equation 3.5. After determining n, K_{ur} can be calculated with a single unloading curve of the triaxial test [36]. In general K_{ur} is greater than K in Equation 3.5 and Duncan (1980) suggests that K_{ur}/K can be taken as 1.2 for dense soils, and as approximately 3 for loose soils when the unloading data of the triaxial test is not available. Note that, the overall stress-strain relation of soil subjected to loading followed by unloading demonstrates inelastic behavior with plastic deformation ε_p Figure 3.5.

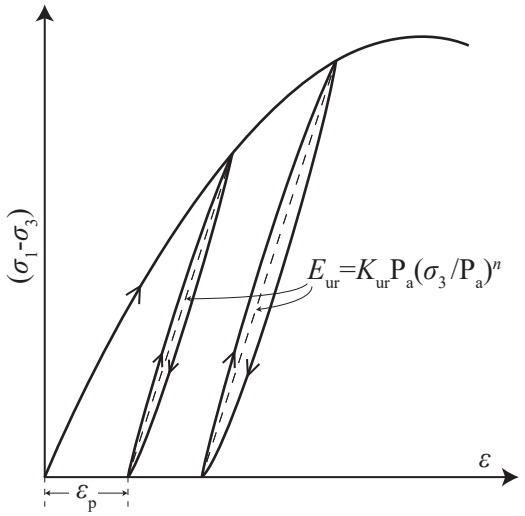

Figure 3.5: Determination of unloading & reloading modulus

Overall, the experimental and numerical processes of determination of each parameter ($K, n, K_{ur}, R_f, c, \phi$) are mentioned. Then, initial modulus E_i can be calculated. E_t, E_{ur} moduli are determined with respect to Equations 3.13 and 3.18. To sum up, the flow chart of the calibration of the Duncan & Chang model is illustrated in Figure 3.6.

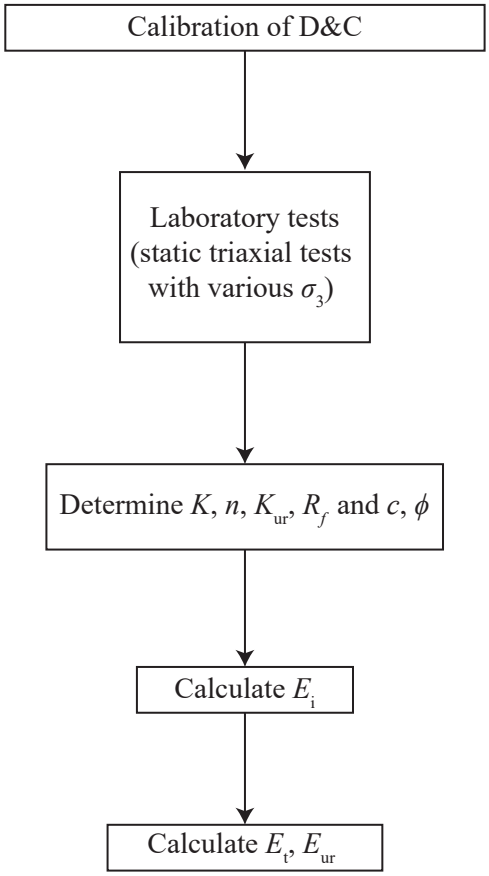

Figure 3.6: Flow chart of D&C

It is important to that D&C is not an energy conservative formulation due to unloading and reloading stages are not accompanied by energy dissipation [39].

3.3 Modifications of Duncan & Chang

Although D&C's hyperbolic elastic model dates to 1970, it is still widely used as a soil material model since its parameters can be easily obtained. Even if testing is not possible, one can get these parameters from literature. This prevalent method has

evolved over time. Related alterations are presented in Table 3.1:

Table 3.1: Comparison of D&C versions

Date	Poisson's ratio (ν) & Bulk modulus (B)	Friction angle (ϕ)
1970 [10]	Constant	Constant
1972 [40]	$\nu = \nu_0 - \Delta\nu \log(\frac{\sigma_3}{P_a})$	Constant
1980 [36]	$B = K_b P_a (\frac{\sigma_3}{P_a})^m$	$\phi = \phi_0 - \Delta\phi \log(\frac{\sigma_3}{P_a})$

Duncan and Chang (1970) [10], original version, is the most widely-used method in which Poisson's ratio, bulk modulus, and friction angle are constant. All its parameters can be obtained from three triaxial tests with different confining pressure and one unloading curve from one of those triaxial tests. Prediction of model achieves a high degree of accuracy with test results [33]. When failure occurs, tangent modulus assigned to soil is too low because of the high value of stress level. This situation leads to excessive deformation even if the stress change is limited. It is not a robust estimation for the behavior of soil after the peak point of deviatoric stress [33].

The update to the model in 1972 [40], which has linearly varying Poisson's ratio within limited range according to stress state, performed poorly compared with the 1970 model (constant Poisson's ratio) in some studies due to the fact that changing Poisson's ratio drives problems in certain conditions [41]. The 1980 model [36] uses confining pressure-dependent bulk modulus and friction angle. It requires one additional triaxial test to detect friction angle and volumetric strain to calculate bulk modulus. Nonetheless, it was observed that volumetric strain could not be acquired by traditional triaxial test machine except in cases where the soil was saturated. Another limitation of this model is that it utilizes bulk modulus with secant value in place of tangent value [42]. To improve the model, bulk modulus was linked to mean normal stress by Boscardin et al. (1990) that overcame some problems emerging from the calculation of bulk modulus.

Overall, to model the monotonic loading and unloading stages, it was decided to use the original D&C 1970 model in this thesis, for two main reasons. The first reason is that the 1970 model requires fewer parameters to calibrate so it needs fewer tests with a high degree of accuracy. Secondly, all models have some limitations as

mentioned above yet the limitation of the 1970 model (not being able to satisfactorily model the stress-strain relation of soil after the yield point) is not a burden for our implementation goals since soil is not loaded up to its yield point before and during cyclic loading. That scenario is beyond the scope of this thesis study.

CHAPTER 4

BACKGROUND ON SOIL BEHAVIOR UNDER CYCLIC LOADING

In this chapter, the cyclic loading response of a soil, previously subjected to monotonic loading, will be investigated. When soil is exposed to cyclic loading, even if applied stress is less than its plastic yield, in contrast to elastic theory, permanent strain occurs. Permanent strain leads to residual settlement. For instance, a monopile or strip foundation subjected to cyclic loading distributes stresses to the soil that surrounds the structure. Permanent settlement or shift (for a monopile) are perpetual even after loading is removed. Figure 4.1 gives an exemplary drawing of a monopile and strip foundation under cyclic load. Forces acting on those structures and the stress response of the soil are also demonstrated.

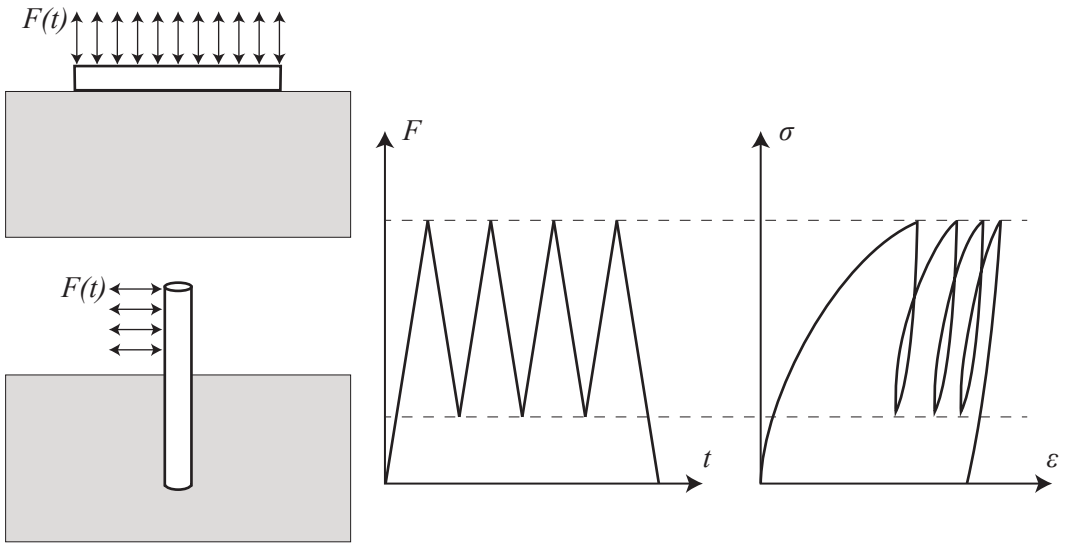

Figure 4.1: Monopile and foundation subjected to cyclic loading

4.1 Soil Response to Cyclic Loading

Prediction of plastic deformation for granular materials is challenging for highway pavements, railway structures, foundations of offshore and onshore wind turbines, cyclically hydrostatic loaded silos, hydraulic structures, machine foundations and all the other cyclically loaded structures that interact with unbound granular materials (UGM). Rutting arising from permanent deformation reduces the performance of structures which leads to economic drawbacks and diminished quality of experience. This phenomenon demands an understanding of elastic and plastic behavior of subgrade soils in various surrounding environments. Besides external effects (loading type, frequency, amplitude), internal factors (aggregate size, distribution, shape and strength, moisture content, relative density, stress history, drainage condition and permeability) related with a soil are also crucial for comprehending soil behavior under cyclic loading [43, 44, 15, 17].

4.1.1 Loading Types & Frequency

There are two different cyclic loading types in terms of loading direction, one-way and two-way loading. If the loading sign changes during cycles, it is called two-way loading. If the loading sign is constant, it is one-way loading. To express this mathematically, Equation 4.1 can be stated

$$R = F_{min}/F_{max} \tag{4.1}$$

where R is the cyclic loading ratio, F_{max} is maximum force and F_{min} minimum force [43, 45]. It is also illustrated in Figure 4.2.

For one-way loading, the value of loading ratio is within the range of $0 \leq R \leq 1$ and for the two-way loading, it is within the range of -1 $\leq R < 0$. In some one-way loading cases, F_{min} may not be zero. For those experiments, there is a constant load on the soil q_{min} (minimum deviatoric stress) such as that created by the weight of triaxial test device loading lid.

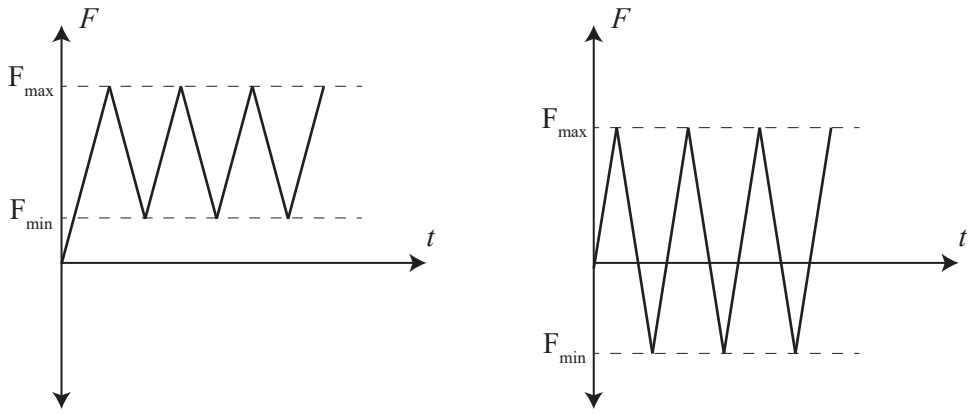

i. One-way loading ii. Two-way loading

Figure 4.2: Loading types

Cyclic loading is repeated application of force, stress, or pressure with a particular pattern of size, direction and frequency in which inertia force is ignored whereas, in dynamic load, which is faster (higher frequency) than cyclic loading, inertia has effects on the mass [43].

For drained and undrained triaxial test, Shenton (1978) and Kokusho et al. (2004) have reported that effects of dynamic loading are not observed in frequency range of 0.1 Hz $\leq f \leq$ 30 Hz [46, 47]. On the contrary, several studies state that there is observable limit for dynamic inertia effect and it is $f >$ 5 Hz [3], and $f >$ 1 Hz [48].

Furthermore, for saturated or partly-saturated soils, load frequency has another effect due to accumulated pore pressure. Increased load frequency leads to intensified pore water pressure without dissipation during subsequent cycles. For a high number of load cycles, it is observed that permanent deformation increases [43].

4.1.2 Varying Load Amplitude

In most cases, the structure is exposed to varying load amplitude. Cumulative permanent deformation caused by such loading can be estimated using two distinct approaches, time-hardening and strain-hardening, as shown in Figure 4.3.

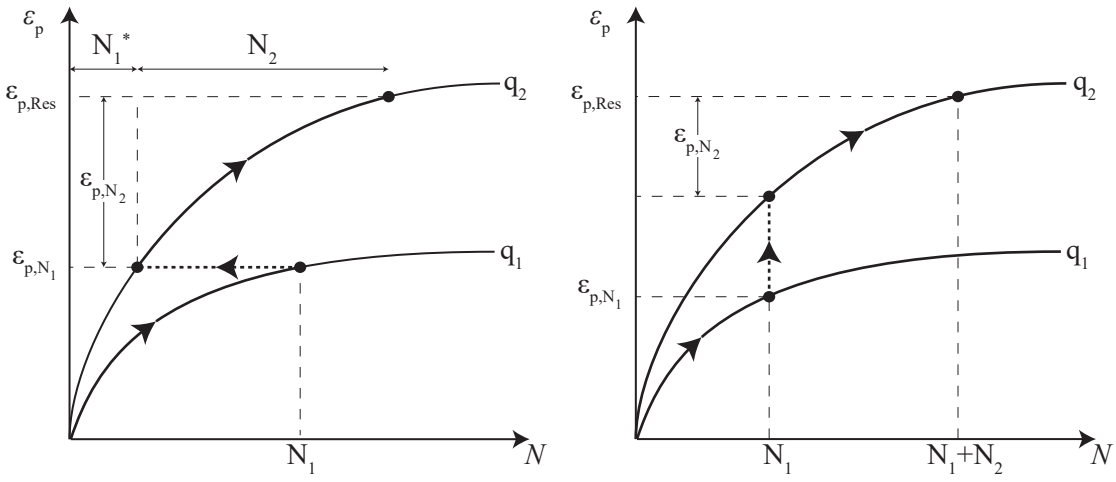

i. Time-Hardening ii. Strain-Hardening

Figure 4.3: Comparison of methods to estimate effects of varying load amplitude

4.1.2.1 Time-Hardening Method

The time-hardening method assumes that N_1 cycles of q_1 deviatoric stress generate ε_{p,N_1} plastic strain. After that, if N_2 cycles of q_2 deviatoric stress are applied, ε_{p,N_1} from the first sequence is converted to N_1^* cycles with respect to parameters of q_2 deviatoric stress. Lastly, total permanent strain is calculated by summing permanent strain from N_1^* and N_2 cycles on the q_2 deviatoric stress curve. Estimation using this method is more successful than when the applied stress of specimen shows an increasing trend [49].

4.1.2.2 Strain-Hardening Method

The strain-hardening method simply expresses that cumulative permanent strain of N_1 cycles of q_1 deviatoric stress and N_2 cycles of q_2 deviatoric stress are calculated as $N_1 + N_2$ on the ε vs. N curve for q_2. Thus, calculated cumulative permanent strain is independent of magnitude of q_1 deviatoric stress. This procedure operates effectively when the loading amplitude of cycles is decreasing [49].

Findings of Poulsen and Stubstad [50] indicate that the time-hardening method performs better in both increasing and decreasing loading amplitude of cycles. However, Tasan [43] observed no significant performance difference between the two methods.

4.1.3 Other Conditions Affecting Permanent Strain

Some other conditions affecting permanent strain can be listed as:

- Permeability: In saturated or partly-saturated soil, permeability has great impact on the drainage of water. Soil with a high permeability coefficient can rapidly discharge excess pore water pressure accumulated by cyclic loading. As pore pressure reduces the bearing capacity of soil, permanent strain increases.

- Relative Density: In relation to compaction, dense soil has less space to be compressed. At the end of cyclic load application, permanent deformation in dense soil (high relative density) is less than in loose soil. In connection with pore pressure, loose soil has spare inter-granular space in which pore water pressure accumulates [43]. Hence, from both compaction and pore pressure viewpoints, high relative density leads to less permanent deformation.

- Moisture Content: Increased water content has a lubricating effect between soil grains. It is observed that even in the absence of excess pore pressure, relatively small amounts of moisture cause large permanent deformation [51]. Saturated soil samples have more considerable permanent strain in comparison with partly saturated samples [52]. As a result of these, high water saturation combined with low permeability is unfavorable in terms of permanent strain [44].

- Density: It is strongly related to compaction degree of soil. The higher the density, the higher the resistance to permanent strain [44].

- Stress History: For every load cycle, soil is compacted and the stiffness of the soil grows. As a consequence of this, permanent strain diminishes for subsequent cycles.

- Grading: Compaction and grading have a close relation. With the same compaction degree, increase of relative density by grading brings better resistance to permanent deformation [44]. Furthermore, research on permanent deformation reveals that grading is more significant than degree of compaction in densely compacted samples [53, 54].

- Aggregate Size: As the amount of fine soil particle increases, permanent deformation decreases [44]. Moreover, resistance to permanent deformation is better in angular aggregates compared to round aggregates, due to particle interlock in which shear resistance of angular particles is superior to that of round particles [44].

4.2 Behavior Types of Cyclic Loaded Soil

Every load cycle attempts to shuffle the position and direction of soil grains which leads to spatial rearrangement of soil particles. Different conditions of soil and its environment cause distinct soil behavior [43]. In the literature these different behaviors have been categorized with three main terms illustrated in Figure 4.4 [17].

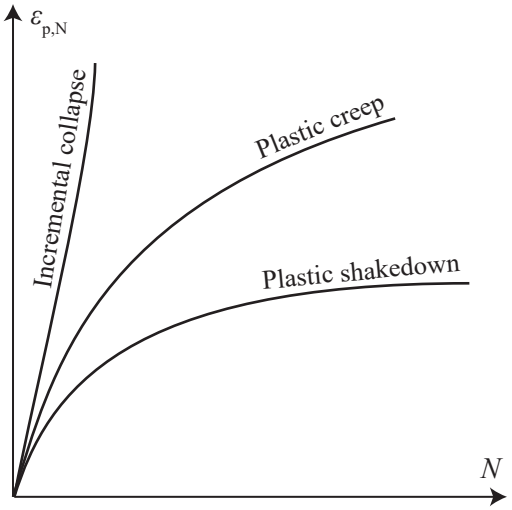

Figure 4.4: Behavior types of cyclic loaded soil

4.2.1 Plastic Shakedown

In plastic shakedown, soil responds as a plastic for a certain number of cycles. After that, the soil behavior becomes elastic (resilient), permanent strain is observed as zero, and cumulative permanent deformation becomes constant. This type of behavior states that for a given system, permanent strain is within the tolerable range to ensure design is resistant to a high number of load cycles. By virtue of absorbing frictional

energy without being crushed or softened, position of aggregates settle for the last cycles of loading. It is important to note that rate of plastic strain relies particularly on stress level [55].

4.2.2 Incremental Collapse

Incremental collapse demonstrates a progressive increase of plastic strain rate at every subsequent load cycle. Permanent deformation does not stop. Soil softening and aggregate crushing occur in this behavior. Grain strength and energy absorption capacity are not sufficient for the applied stress level. If soil undergoes incremental collapse behavior, structural failure will probably be observed [55].

4.2.3 Plastic Creep

Plastic creep is the intermediate response that is placed between plastic shakedown and incremental collapse. Throughout the initial cycles, rate of permanent strain is higher, whereas it gradually decreases in the following cycles. For the late cycles, permanent strain rate, which depends on soil condition and stress level, becomes constant. As a consequence of the constant permanent strain rate, cumulative plastic deformation exhibits a linear increase. Aggregate energy absorption is lower in this behavior than in plastic shakedown [17].

4.3 Prediction of Permanent Deformation

Throughout the years, scientific methods for deformation estimation of granular materials have evolved. One of the earliest approaches to estimating deformation is to limit the vertical strain within acceptable levels for specific cyclic load repetitions [56]. It is basically the elastic analysis which determines the corresponding layer thickness for the permissible vertical strain without allowing excessive rutting. This relation is established using the California bearing ratio (CBR) which is a widely used experimental test for pavement design. The limiting strain method was improved further to two-layered elastic design that embodies an asphalt layer with a granular sublayer

[57]. However, these elastic methods have the limitation that they can't compute the permanent deformation of the layers [58]. In addition, granular materials don't demonstrate purely elastic behavior, and permanent deformation is always observed along with resilient strain due to post-compaction of soil [55].

Different than the previously mentioned studies which are based on static tests, Haynes [59] and Barksdale [52] proposed models built on laboratory cyclic triaxial test to predict performance of granular materials at sublayers. Currently, permanent strain prediction methods for granular materials can be listed as explicit, implicit and shakedown methods [60]. Explicit approaches employ pre-determined correlation to estimate residual strain with various parameters. In this study, explicit models are investigated in detail. Implicit approaches are based on incremental $\sigma - \varepsilon$ constitutive relation that they progressively compute cyclic reaction of granular material. Implicit methods could utilize elasto-plastic or nonlinear elastic relation to soil [20, 18, 61]. Lastly, shakedown theory determines whether a system is stable or not under the applied stress. It asserts that if the stress level is below a specified threshold, cumulative permanent strain will be balanced after a particular number of cycles [55, 17, 62, 19].

4.3.1 Explicit Method

One of the conventional approaches to forecast permanent deformation of granular materials is classified as the explicit method, also known as the analytical or the empirical method. In the explicit method, the calculation of the accumulated deformation of granular materials is regarded like the viscosity with the number of cycles (or other variables) in place of the time [3]. Several correlations are provided to predict plastic strain empirically. Some studies present the relation of permanent strain (ε_p) with applied stress (q) to the specimen [63, 46]. Moreover, one study [16] associates resilient (elastic) strain (ε_e) to permanent strain (ε_p), yet Sweere [15] could not prove the relation.

Furthermore, another study linked permanent deformation to both the number of loading cycles (N) and applied stresses [64]. On the other hand, a majority of studies craft this relation as cumulative plastic strain to the number of cycles [65, 66]. This is one of the prevailing methods to estimate permanent deformation which is related to the

number of load cycles.

4.3.1.1 Plastic Deformation vs. Number of Cycle

The relationship between number of load cycles and cumulative permanent deformation strain is established and it has become one of the most employed correlations describing the cumulative plastic strain as a function of cycle number. Researchers have implemented different mathematical functions to describe the relation. The first function is a semi-logarithmic approach that defines:

$$\varepsilon_{p,N} = a_1 + a_2\, log(N) \tag{4.2}$$

Cumulative permanent strain is proportional with the logarithm of the number of cycles [52, 46, 67, 66]. The second function is a log-log approach:

$$\varepsilon_{p,N} = a_1 N^{a_2} \tag{4.3}$$

The logarithm of cumulative permanent strain is proportional with the logarithm of the number of cycles [49, 58, 68, 15, 69, 70, 43]. Thirdly, Wolff & Visser (1974) propose [71]:

$$\varepsilon_{p,N} = (a_1 N + a_2)(1 - e^{-a_3 N}) \tag{4.4}$$

Moreover, Paute et al. (1996) offer [72]:

$$\varepsilon_{p,N} = a_1\Big(1 - \Big(\frac{N}{100}\Big)^{-a_2}\Big) \tag{4.5}$$

Lastly, Cerni et al. (2012) present [60]:

$$\varepsilon_{p,N} = a_1 + a_2 N - a_3\, e^{-a_4 N} \tag{4.6}$$

where a_1, a_2, a_3 and a_4 are regression parameters for all equations (4.2, 4.3, 4.4, 4.5, 4.6). Cerni et al. (2012) compared these explicit models using their determination coefficients (R^2) that measures fitness of regression to experimental data [60]. Equation 4.2, 4.3, 4.5 and 4.6 have fitted with test results over 95% R^2. In this study, the log-log approach (Equation 4.3) is implemented due to its simplicity and being a widely preferred model.

4.3.1.2 Log-Log Approach

Further investigations on $\varepsilon_{p,N} = a_1 N^{a_2}$ reveal that for the first cycle ($N = 1$), Equation 4.3 produces $a_1 = \varepsilon_{p,\ N=1}$ which depicts a_1 is equal to permanent strain at the end of the first cycle. This parameter is highly correlated with soil properties and the stress level. [49, 67, 68, 15, 66, 43].

On the other hand, a_2 in Equation 4.3, is independent of stress state and the dry density of soil [49, 58]. Parameter a_2 increases only with moisture content [69]. It is constant for a given water content. Different levels of deviatoric stress do not lead to changes in the value of a_2 [65]. If it is assumed that moisture content is equal for all soil sections that are taking consideration, constant and permanent a_2 value can be utilized in the model.

Parameter a_1 is called the "Intercept" or the "Intercept coefficient," whereas parameter a_2 is known as the "Slope" or "Slope coefficient." In Figure 4.5, an exemplary data set of cumulative plastic strain to number of loading cycles plot is illustrated. The red dashed line is fitted with the least-squares approach in regards to Equation 4.3. Furthermore, Figure 4.6 is the log-log scale form of Figure 4.5, with the same data set. The red dashed line also represents Equation 4.3. Moreover, in Figure 4.6, the **slope** of the red line corresponds to parameter a_2, the **intercept** distance at which the red line intersects the y-axis is equal to parameter a_1.

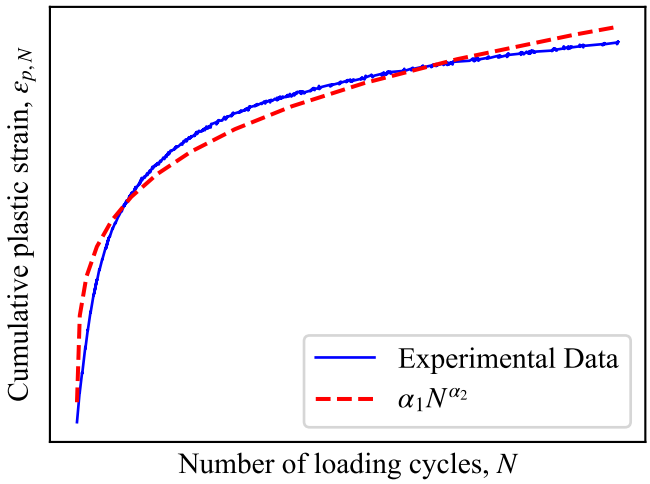

Figure 4.5: Cumulative plastic strain vs. number of load cycles

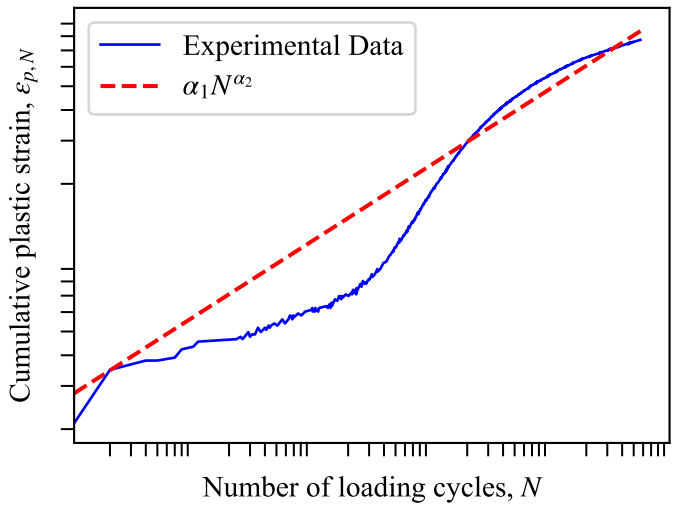

Figure 4.6: Log-log scaled cumulative plastic strain vs. number of load cycles

CHAPTER 5

EXPLICIT CYCLIC DUNCAN CHANG MODEL

In this chapter, a new simplified model (Explicit Cyclic Duncan Chang) that merges nonlinear elastic constitutive relation of soil (Duncan & Chang model in Chapter 3) with explicit cyclic behavior (log-log scaled explicit permanent deformation approach in Chapter 4) is presented. Then, the implementation process of the proposed material model to a finite element solver is elaborated. The verification of the implementation of the D&C model is done. Furthermore, a 3D monopile subjected to cyclic horizontal loading is analyzed using the Explicit Cyclic Duncan Chang (ECDC) model and thereafter the analysis is compared with experimental test results.

5.1 Representation of ECDC

ECDC is a cycle-dependent explicit method with similar representation of the Maxwell model. It resembles a time-dependent creep behavior notion that in the literature has already been associated with permanent deformation accumulation characteristics of soil, such as the densification model [73, 21] and accumulation model [74].

To implement ECDC into ANSYS Usermat as subroutine, its constitutive relation needs to be written in incremental stress form. Thus, the following equation presents the fundamental representation of ECDC:

$$d\sigma^{n+1} = C_{\Delta q^n} : (d\varepsilon^{n+1} - d\varepsilon_p^n) \tag{5.1}$$

where $d\sigma^{n+1}$ is the stress increment, C is the material tangent modulus, $d\varepsilon^{n+1}$ is the strain increment and $d\varepsilon_p^n$ is the explicit plastic strain increment in the explicit

stage. During the monotonic loading stage, $d\varepsilon_p^n$ is zero and C is deviatoric stress (Δq) dependent (details in Chapter 3). In the explicit step, explicit plastic strain increment ($d\varepsilon_p^n$) becomes non-zero and calculated explicitly with $\varepsilon_p = a_1 N^{a_2}$ (details in Chapter 4). During explicit calculation (cyclic stage), $d\sigma$ becomes zero; thus, strain increment for this step equals the explicit plastic strain increment ($d\varepsilon_p^n = d\varepsilon^{n+1}$).

5.1.1 Monotonic Loading - First Cycle

As illustrated in the deviatoric stress to strain plot in Figure 5.1, a soil sample in triaxial text device is monotonically loaded in 15 stress increments. Subsequently, one unloading step completes the first cycle. Soil response for loading is nonlinear, whereas its response to unloading is linear as D&C. This loading and unloading constitutes the first cycle and it is an implicit step that σ-ε constitutive relation is utilized.

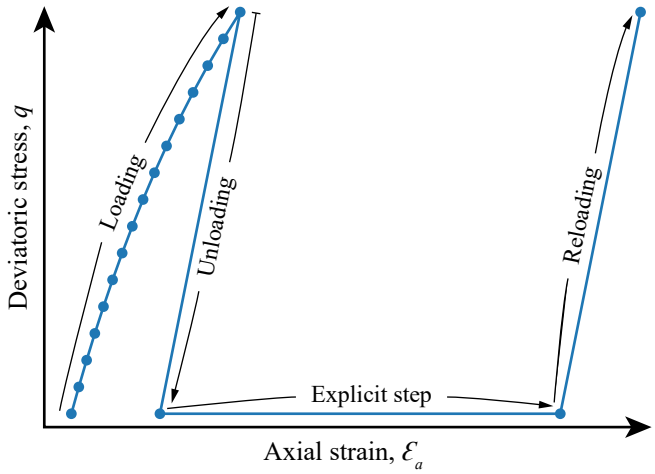

Figure 5.1: Stress-strain curve of monotonic and cyclic loading process

Furthermore, the rheological device of ECDC in the first cycle is provided in Figure 5.2. It has a nonlinear spring and a frictional slip device to yield permanent strain in the monotonically loaded first cycle (slip device is utilized to represent permanent strain for illustrative purpose, in this case it is not related to general plasticity theory). For this stage, the switch is off; the dashpot is not connected to the system. Thus, it does not contribute to the accumulation of the permanent strain. The rheological device is monotonically loaded (up to q) and unloaded (to 0), which produces the

permanent strain of the first cycle on the slip device corresponds to parameter a_1 in Equation 4.3.

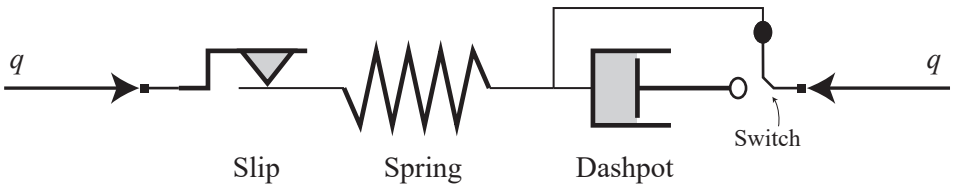

Figure 5.2: Monotonic loading stage

5.1.2 Explicit Step - Rest of the Cyclic Loading

After the first cycle is completed, the rest of the cycles are explicitly calculated in order to limit error accumulation and simplify the required computational process. In Figure 5.3, the switch is on; the dashpot is active. It is cycle-dependent as distinct from a standard dashpot which is time-dependent. Constant stress is applied to the rheological device; therefore, strain in spring and slip is identical as in the monotonic loading/first cycle. The dashpot delivers permanent strain for $N-1$ cycles with respect to $\varepsilon_{p,N-1} = a_1(N-1)^{a_2}$ function. a_1 is determined from the first cycle, a_2 is detected from cyclic triaxial tests (details in Section 5.2). Overall, the cumulative permanent strain from the system can be estimated with parameters obtained. This explicit step is also called "accumulation" in the literature [3].

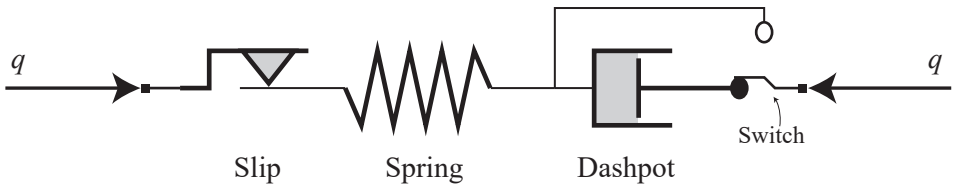

Figure 5.3: Cyclic loading stage

5.1.3 Reloading

If the objective of the analysis is to detect total strain (permanent strain + elastic strain), an additional reloading step is required. It uses D&C's linear reloading modulus which is identical to unloading modulus (if q_{max} in reloading exceeds q_{max} in the first cycle, stress-dependent nonlinear modulus of D&C should be utilized). The reloading step, similar to unloading of the first cycle, is linear elastic analysis as mentioned in Chapter 3. Elastic strain (called resilient strain in geomechanics) is calculated and added to the previously found plastic strain to acquire total strain. Moreover, the reloading stage provides a more stable system following to explicit step. In Figure 5.4, the first cycle, the explicit step of cyclic loading, and the reloading step are illustrated distinctly.

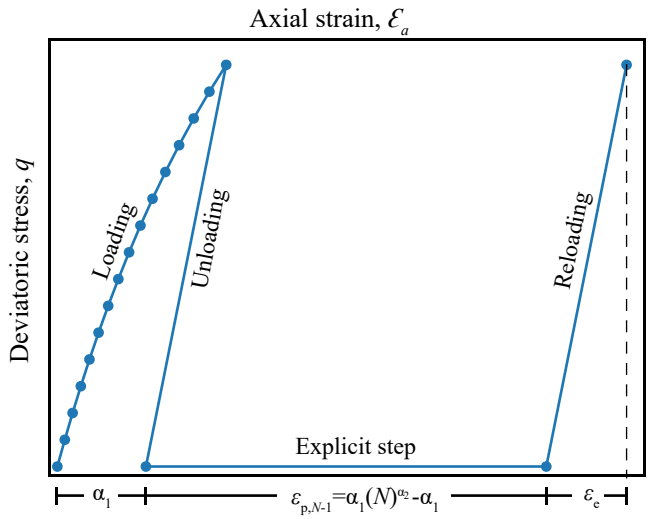

Figure 5.4: Details of all loading steps

Gravity loading (for initial state of soil), D&C loading, D&C unloading, explicit stage and D&C reloading steps are specified by "load step number" (ldstep parameter) both in the input file of ANSYS and Usermat.

It is worthwhile to mention that an advantage of ECDC over other explicit models is that it does not require additional plastic yield surface control. In particular situations, certain soil elements might have stress states which lie in outside of yield surface which is not possible in terms of plasticity theory. This situation necessitates additional plastic strain calculation (different than explicit step) as some studies

have accomplished [3]. On the other hand, D&C that is utilized in loading-unloading and reloading stages innately includes plasticity control by virtue of its algorithm discussed in Chapter 3.

Moreover, in contrast to some hypoplastic-explicit methods, the first cycle is sufficient for ECDC. Since the deformation in the explicit step can be readily estimated directly after the first cycle. In certain complex systems that are solved using the finite element method, interfering with the explicit step might lead to undesirable outcomes [3]. Both monotonic loading at the first cycle and reloading stage at the last cycle are sufficient to redistribute stress as priori and posteriori steps of explicit step in ECDC.

5.2 Determination of Explicit Parameters

In this section, as an example of the determination of explicit parameters, ECDC related parameters of Berlin sand [43] are calculated. It is poorly graded, round-shaped sand with $\rho_{d,min} = 1.52\ g/cm^3$, $\rho_{d,max} = 1.88\ g/cm^3$, $\rho_s = 2.65\ g/cm^3$, $C_u = 2.9$, $w_{opt} = 9.5\ \%$ and $\rho_{opt} = 1.79\ g/cm^3$. In addition, Duncan & Chang parameters are given in Table 5.1. Moreover, these parameters are utilized during the monopile calculation later in this chapter.

Table 5.1: D&C parameter of Berlin sand

Relative Density	ϕ	R_f	K	K_{ur}	n	c
77 %	40.4	0.90	1398.5	1853.5	0.875	0

Cyclic triaxial test is conducted with two different cyclic load ratios (X) which is the ratio of cyclic deviatoric stress (q) to static deviatoric stress at failure ($(\sigma_1 - \sigma_3)_f$) which can be calculated with Mohr-Coulomb yield criterion with Equation 3.6. Both $X = 0.58$ and $X = 0.37$ tests have equal $\sigma_3 = 100\ kN/m^2$ confining pressure. $X = 0.58$ corresponds to $\Delta q = 237\ kPa$, whilst $X = 0.37$ has $\Delta q = 153\ kPa$ deviatoric stress amplitude. "Cumulative permanent deformation" vs. applied "load cycle number" results of cyclic triaxial test with different cyclic load ratio are provided in Figure 5.5. Moreover, a simple cyclic triaxial test scheme is also illustrated in Figure 5.6. In those figures, q is deviatoric stress $(\sigma_1 - \sigma_3)$ and Δq represents absolute load

amplitude ($q_{max} - q_{min}$). Lastly, q_{max} is deviatoric stress at the crest of the load cycle whereas q_{min} is at the trough of the load cycle.

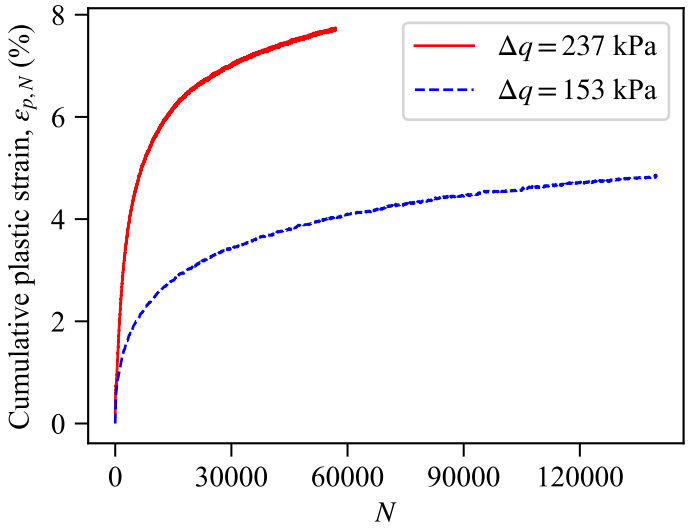

Figure 5.5: Cyclic triaxial test results with different Δq

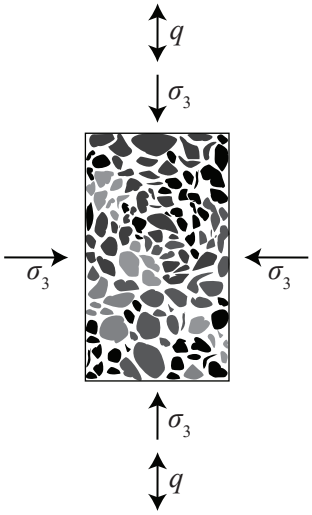

Figure 5.6: Cyclic triaxial test scheme

5.2.1 Determination of Intercept Coefficient

To determine the corresponding value of a_1, it is necessary to run the complete first cycle implicitly. As previously mentioned in Chapter 3, nonlinear inelastic constitu-

tive relation of D&C is implemented. Since the D&C parameters already detected in Table 5.1, the static triaxial unit model with 1x1x1 m dimensions is analyzed in ANSYS by calling user modified Usermat which has D&C loading and unloading algorithm. In Figure 5.7, details of the first cycle for $\Delta q = 237\ kPa$ is demonstrated. Loading is divided into 15 increments to exhibit nonlinearity of stress dependent modulus. After that, soil is unloaded with one step since it has linear tangent modulus. The strain that remains when the analysis is concluded is permanent strain for the first cycle $\varepsilon_{p,N=1}$, also known as parameter a_1.

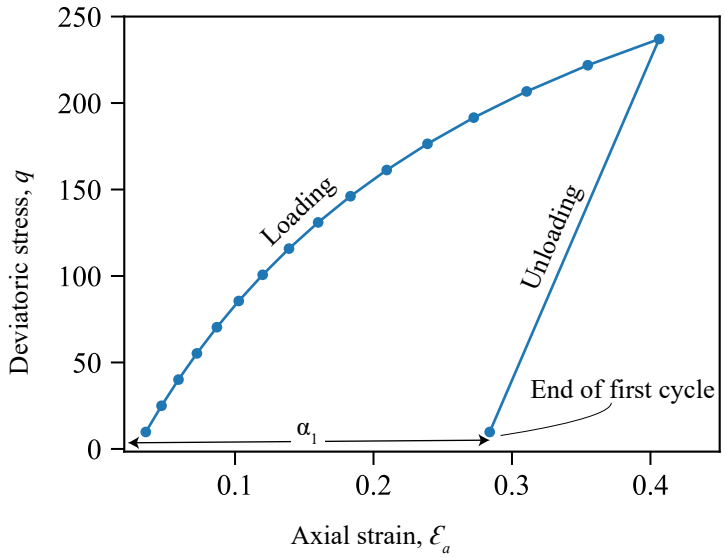

Figure 5.7: First cycle of $\Delta q = 237\ kPa$

Cumulative permanent deformations in the major axis for $\Delta q = 237\ kPa$ and $\Delta q = 153\ kPa$ are presented in Figures 5.8 and 5.9, respectively.

5.2.2 Determination of Slope Coefficient

After determining a_1, parameter a_2 is calculated by nonlinear regression with the least-squares method. In contrast to a_1 which is stress-dependent parameter, a_2 is non-stress dependent which is constant and unique to soil for same moisture content as explained in Section 4.3.1.2. a_2 is obtained as 0.310 for analysis that is conducted on Berlin sand with same water content in the following sections [43]. Figures 5.10 and 5.11 contain results of a_2 from cyclic triaxial tests for $\Delta q = 237\ kPa$ and $\Delta q =$

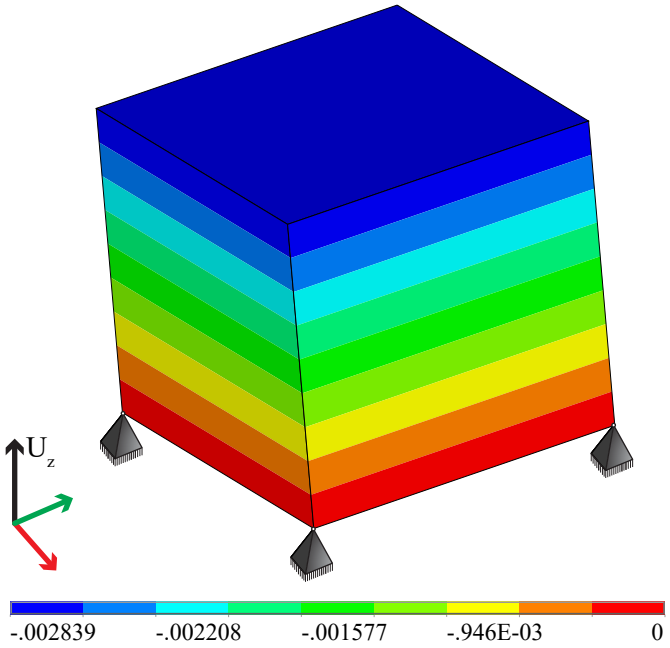

Figure 5.8: Displacement at the end of the first cycle, $\Delta q = 237\ kPa$

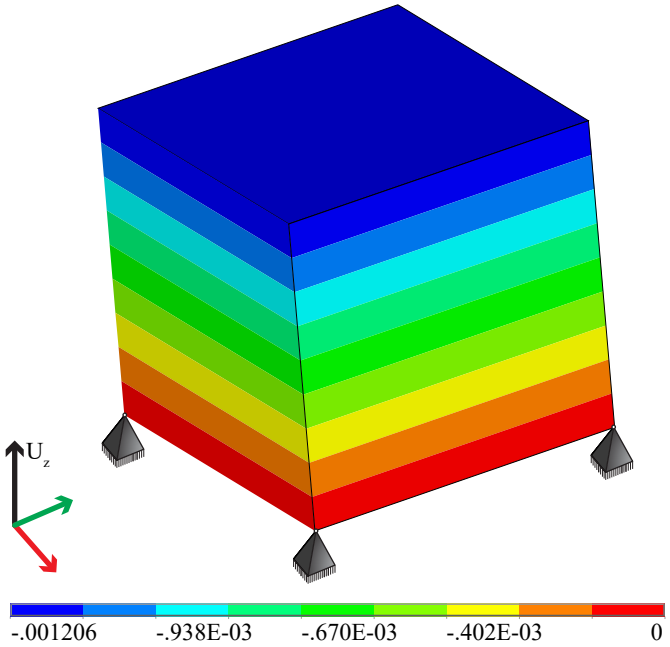

Figure 5.9: Displacement at the end of the first cycle, $\Delta q = 153\ kPa$

$153\ kPa$.

Interpreted parameters of cyclic loading analysis are presented in Table 5.2

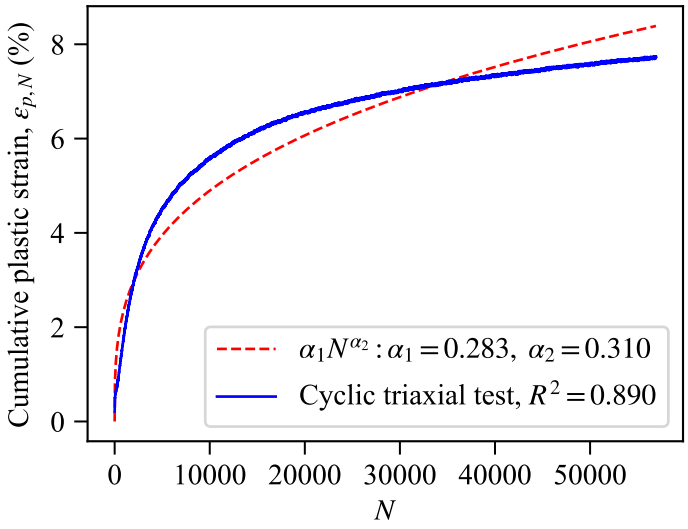

Figure 5.10: Nonlinear regression of cyclic triaxial test data for $\Delta q = 237\ kPa$

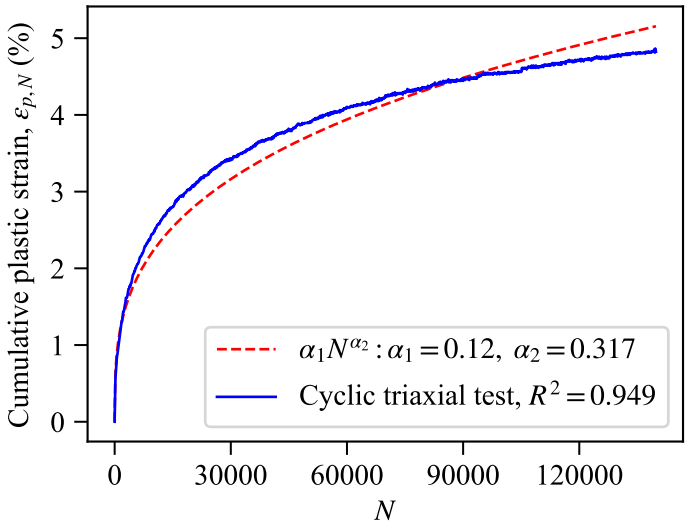

Figure 5.11: Nonlinear regression of cyclic triaxial test data for $\Delta q = 153\ kPa$

Table 5.2: Cyclic triaxial test results

	$a_1 N^{a_2}$	
	a_1	a_2
$X = 0.37$	0.120	0.317
$X = 0.58$	0.283	0.310

5.3 ANSYS - Usermat Implementation

In this study, a unique material model is proposed. To test this constitutive relation, the continuum body of soil domain is solved using the Finite Element Method. Especially for 3D geometry, writing code for meshing the body and solving boundary value problem with the finite element solver from scratch are arduous tasks. ANSYS is a powerful FEM solver with pre- and post-processing capabilities through the ANSYS parametric design language (APDL), which is the input language of ANSYS with the ability of parametric geometry design, meshing, storing data and controlling analysis steps [75]. Moreover, it has an open structure that permits the user to implement customized subroutines and to link those subroutines back to the ANSYS [76]. Thereby, a new material model or unique element type written by the user in C or Fortran can be implemented through ANSYS. This feature is called the user-programmable features (UPFs), and "usermat.f" is the subroutine file that contains material behavior. For this study, we have written our constitutive relation into Usermat file.

During the solution stage, Usermat which establishes the σ-ε relation is called for each material integration point of elements [76]. ANSYS provides stress, strain, state variables, and strain increment to the Usermat for every time step. After that, Usermat updates stress, state variables, and the material Jacobian matrix according to constitutive relation that the user-specified. A simple scheme of how Usermat runs under ANSYS is illustrated in Figure 5.12. Those variables are categorized as input, output, and input-output arguments with regards to its order in updating scheme and the variable parameters represent stress, strain, strain increment, state variable, and stiffness matrix are given in parentheses [76].

- Input arguments:

  Strain (*Strain*) represents true logarithmic strain (ε) at time step n.

  Strain increment (*dstrain*) is current increment of $d\varepsilon$.

- Input-output arguments:

  Stress (*stress*) assesses Cauchy stress (σ) both at time n and $n+1$.

State variable (*statev*) is provided by user through input file of APDL with command TB, STATE at time step n. In Usermat, this parameter can be updated and stored for further usage at time step $n + 1$.

- Output arguments:

  Material Jacobian matrix (*dsdePl*) is the stiffness matrix with incremental stress and strain notation ($d\sigma_{ij}/d\varepsilon_{ij}$). ANSYS requires it to be updated for nonlinear analysis.

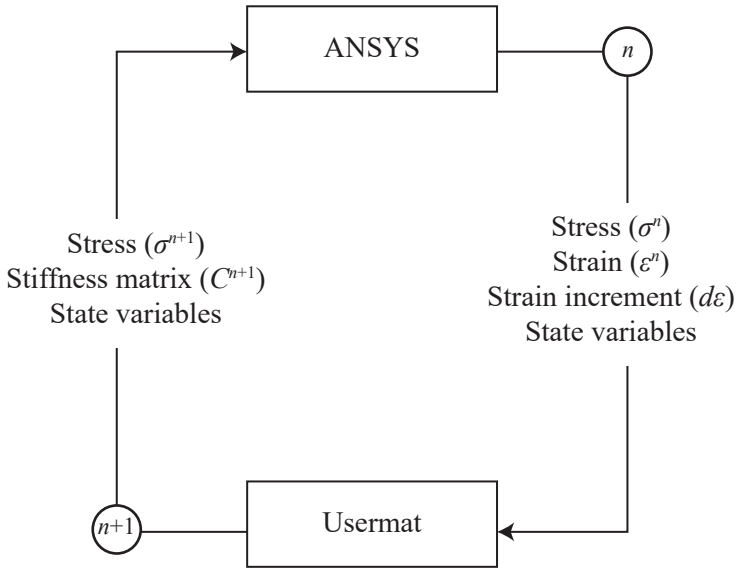

Figure 5.12: ANSYS-Usermat working scheme

Overall, the user-defined Usermat file based on Box 2 algorithm is created to implement the ECDC material model with respect to above-mentioned principles of UPFs. $\sigma - \varepsilon$ constitutive relation of ECDC is tested and debugged for a single element to prepare for full-scale 3D analysis. Then, this Usermat file is linked to ANSYS. For finite element discretization, the inherently available 3D, 8-node solid hexahedral element of ANSYS (SOLID185) is employed.

Note that in this study, the index sorting order of stress and strain matrices are identical with ANSYS's notation which is [11,22,33,12,23,13] whereas ABAQUS, is another FEM solver software, uses [11,22,33,12,13,23] indices sorting. Moreover, as ANSYS states in its help manual [76] that it uses the Voigt notation. However, when

the exemplary Usermat.f code provided by ANSYS is investigated, it is evident that ANSYS internally calculates $2\varepsilon_{12}$, $2\varepsilon_{23}$, $2\varepsilon_{31}$ as ε_{12}, ε_{23}, ε_{31}, respectively. Therefore, there is no further need to multiply ε_{12} by 2.

Box 2: ECDC algorithm

1. Calculate the stiffness matrix of each hexahedral element of meshed body.
   $k^e = \int_{B^e} B^T[C]B \, \mathrm{d}V$ ($[C]$ is provided in Usermat.f file)
2. Construct global stiffness matrix k_{global} and compute matrix inversion k_{global}^{-1}.
3. Calculate nodal displacements d^e by
   $d^e = k_{global}^{-1} \, \Delta f$ (in which Δf is load increment)
4. Compose strain field matrix.
   $\varepsilon = Bd^e$
5. Check the loading type:
   (a) If it is a cyclic loading stage:
      i. Calculate permanent strain increment $d\varepsilon_p$.
         $d\varepsilon_p = a_1 N^{a_2}$
      ii. Compute contribution of permanent strain increment as return mapping algorithms.
         $d\sigma_p = -C : d\varepsilon_p$
      iii. Calculate stress matrix in Voigt notation on every Gauss integration point.
         $\sigma^{n+1} = \sigma^n + C : (d\varepsilon^{n+1} - d\varepsilon_p^n)$
         where $\sigma^{n+1} - \sigma^n = d\sigma^{n+1}$.
   (b) If it is a monotonic loading (loading, unloading or reloading):
      i. Calculate stress matrix in Voigt notation on every Gauss integration point.
         $\sigma^{n+1} = \sigma^n + C : d\varepsilon$ (This step takes place in Usermat.f)
         where $\sigma^{n+1} - \sigma^n = d\sigma$ equality holds.

5.3.1 Verification of Linear Elasticity Algorithm in D&C

The initial step of D&C (1970) is isotropic linear elastic as in Eq. 3.11 stress level is zero in the first step. To verify our model, the ANSYS Built-in linear elastic model is compared with Usermat.f, which contains our D&C algorithm written in Fortran programming language. Figure 5.13 is the nodal solution of z-direction displacement of one element under gravity loading solved by Usermat.f and ANSYS Built-in model side by side. SOLID186, which is a 3-D 20-node structural solid element, is utilized as element type. Dimensions of these cubes are $1x1x1\ m$ with $1\ m^3$ volume. For default ANSYS linear isotropic elastic behavior the "MP, EX" and "MP, NUXY" commands are triggered with a value of $E = 44 \cdot 10^7\ P_a$ and $\nu = 0.3$, respectively. To induce Usermat.f, the "TB, USER" command is employed with required parameters for linear elastic algorithm in Usermat.f. For both of these models, gravity load is provided with the "ACEL" command as $g = 9.81\ m/s^2$ and density of material is given with the "MP, DENS" command as $\gamma = 2000\ kg/m^3$. Lastly, nodes where $z = 0$ are fixed with zero displacement for x, y, and z directions.

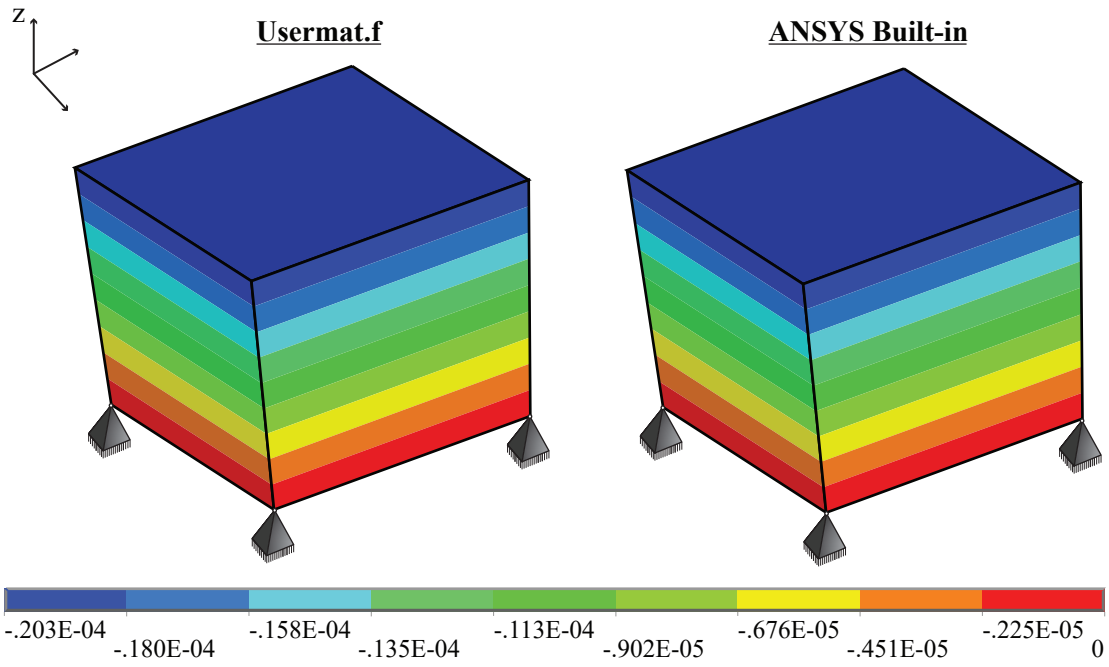

Figure 5.13: Linear elastic comparison of Usermat.f vs. ANSYS built-in model for displacement in the z-direction

Results are compared in x, y, z directions, and displacement of these axes have equal values for both models. Note that direct a comparison of Usermat.f and the ANSYS built-in linear elastic model does not always deliver reliable results since ANSYS tends to solve Usermat.f with a nonlinear solver. For complex geometries, differences in results may occur. Lastly, to demonstrate the correctness of the outcome:

$$mg = 2000 \cdot 1 \cdot 9.81 = 19620\ N,\ 19620/2 = 9810\ N$$

$19620\ N$ is the force due to self-weight of one element calculated by multiplying $\gamma = 2000\ kg/m^3$, $V = 1m^3$, and $g = 9.81\ m/s^2$. 10 of the 20 nodes are fixed in the z-direction, so the others move with the nodal forces from gravitational acceleration. Thus, $19620\ N$ is divided by two to estimate total force on the top four nodes of the element.

$$A = 1\ m^2,\ \sigma = 9810\ P_a,\ \frac{\sigma}{E} = \frac{9810}{44 \cdot 10^7} = 0.223 \cdot 10^{-4}$$

$9810\ N$ is the total force at the top 10 nodes and area A is $1\ m^2$. So, strain in the z-direction can be estimated as $0.223 \cdot 10^{-4}$ which is close to the result in Figure 5.13.

5.3.2 Verification of the Nonlinear Algorithm in D&C

The nonlinearity of the D&C model is based on a stress-dependent elastic modulus that is updated in every increment (step) of solution, as illustrated in Figure 3.1. The changed elastic modulus alters the stiffness matrix (also known as the material Jacobian matrix). For instance, at the beginning of the first step, stress level (S) is zero (before the loading). Consequently, the elastic modulus (E_t) is equal to initial tangent modulus (E_i) (Equation 3.11). By increasing loading, σ_1 becomes larger than σ_3 that leads to a rise in stress level which lowers the elastic modulus. This approach can also be called multilinear hardening in regard to the continuously varying modulus [77]. However, in the literature, it is postulated that if a model has a systematic procedure to update modulus with stress increment, it is preferred to call it hyperbolic rather than multilinear [33]. Nonlinearity of curve is produced by a sequence of straight lines.

Those pieces are generated with tangent modulus values that are assigned to every element at the initiation of each new increment of loading [10]. Thus, in order to achieve a smooth nonlinear stress-strain curve, applied loading to triaxial test sample or complex system needs to be divided into a relatively large number of steps.

At this point, it should be noted that elastic modulus must have a positive value; otherwise, the program would crash during finite element analysis which cannot take zero or negative values. As a consequence, it is not possible to model the behavior of the soil after the peak point of deviatoric stress with D&C since it would require negative values of tangent modulus. For the purpose of verifying our algorithm, the finite element solution is compared with the experimental triaxial test results in [10]. Parameters of the sand used are given in Table 5.3. As the relative density of the soil changes, all parameters vary accordingly. Triaxial tests are carried out with two different relative densities, which are 100 % and 38 %, called dense and loose sand, respectively. These parameters in Table 5.3 differ with respect to the relative density of soil.

Table 5.3: Loose and dense sand parameters (Duncan & Chang 1970)

Relative Density	ϕ	R_f	K	K_{ur}	n	c
38 % (Loose sand)	30.4	0.90	295	1090	0.65	0
100 % (Dense sand)	36.5	0.91	2000	2120	0.54	0

Tests are conducted at 1, 3, and 5 kgf/cm^2 constant confining pressure σ_3 with increasing σ_1 up to Mohr–Coulomb yield strength which varies with related parameters and confining pressures (Equation 3.6). Right above the yield strength, the behavior of soil can be assumed as perfectly plastic.

Triaxial test is taken into consideration as a unit test that describes the constitutive relation of the entire specimen within one element [78]. Therefore, we meshed one finite element with dimension of $1x1x1\ m$ to simulate the triaxial test. It is quarterly modeled owing to symmetry and the element is constrained as illustrated in Figure 5.14.

As the first step, gravity loading is employed with initial tangent modulus. It is simple

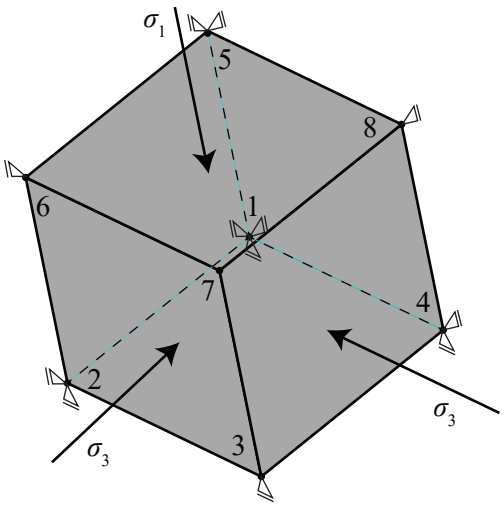

Figure 5.14: Modeling triaxial test

linear elastic analysis. During the following steps, σ_1 is increased in 40 increments and σ_3 is held constant. Stress in the z and x-directions, displacement and strain results of analysis are obtained for Node 7 which is a non-constrained node demonstrated in Figure 5.14.

Outcomes of simulations and triaxial tests are compared in Figure 5.15 and Figure 5.16. Finite element analysis is represented as "Usermat.f", whereas laboratory triaxial tests by Duncan & Chang (1970) are labeled "D&C (1970)". The y-axis is the deviatoric stress (kgf/cm^2), x-axis is the axial strain. At total of six tests are exhibited, three tests for loose sand and three tests for dense soil at constant σ_3 of 1, 3, and 5 kgf/cm^2.

The finite element solution agrees well with the triaxial test results both for the dense and the loose sand. It is also noticed that comparison indicates a better fit for dense soil, and the results are acceptable for loose soil. Not surprisingly, the literature shows a considerable inclination toward this method. Figure 5.15 and Figure 5.16 represent verification of the code for the monotonic loading stage. It should be noted that Usermat.f is capable of calculating the unloading and reloading stages. Moreover, shape of curves are well aligned with triaxial tests. However, comparison of those cases are not illustrated since those analysis are simple linear behavior that can also be calculated easily by hand.

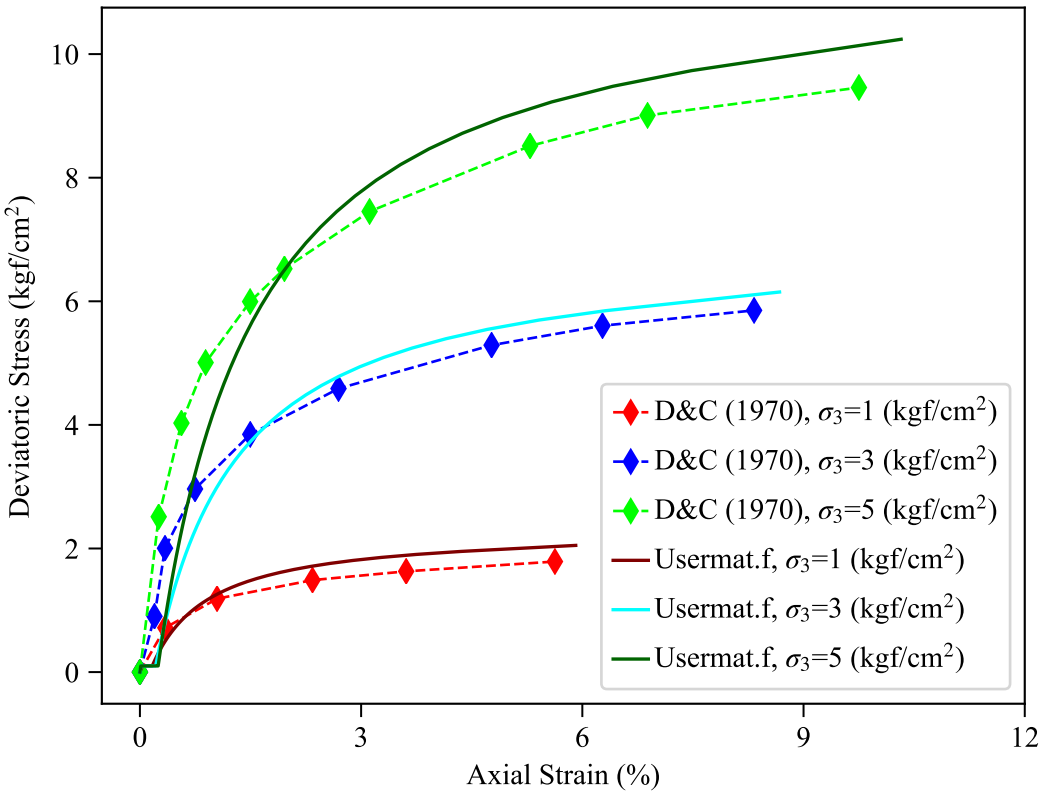

Figure 5.15: ANSYS Usermat.f simulation vs. D&C (1970) triaxial test (loose sand)

5.4 Analysis of A Cyclic Horizontally Loaded Monopile

In this section, the ECDC model is utilized to solve 3D problem of a horizontally cyclically loaded monopile embedded in Berlin sand with a relative density of 0.77. The monopile has diameter of $d = 0.14\ m$, a total length of $l = 3.02\ m$ ($2.41\ m$ is submerged in fully saturated sand), and a pile thickness of $t_p = 0.004\ m$.

The steel pile is modeled as linear elastic with $E = 2.1 \cdot 10^{11}\ N/m^2$ and $\nu = 0.3$. The soil is meshed with 3D 8-node hexahedral solid elements by assigning ECDC as the material model. High-order 3D 20-node solid elements do not have a critical impact on the results in our case. Since 8-node element type requires less computational resources, it is preferred over the high-order element type. Similarly, utilizing an element type with a linear shape function over a quadratic shape function to solve plain strain boundary condition problem with the explicit hypoplastic method reveals that linear shape function is adequate [3, 74, 79]. Furthermore, interaction between

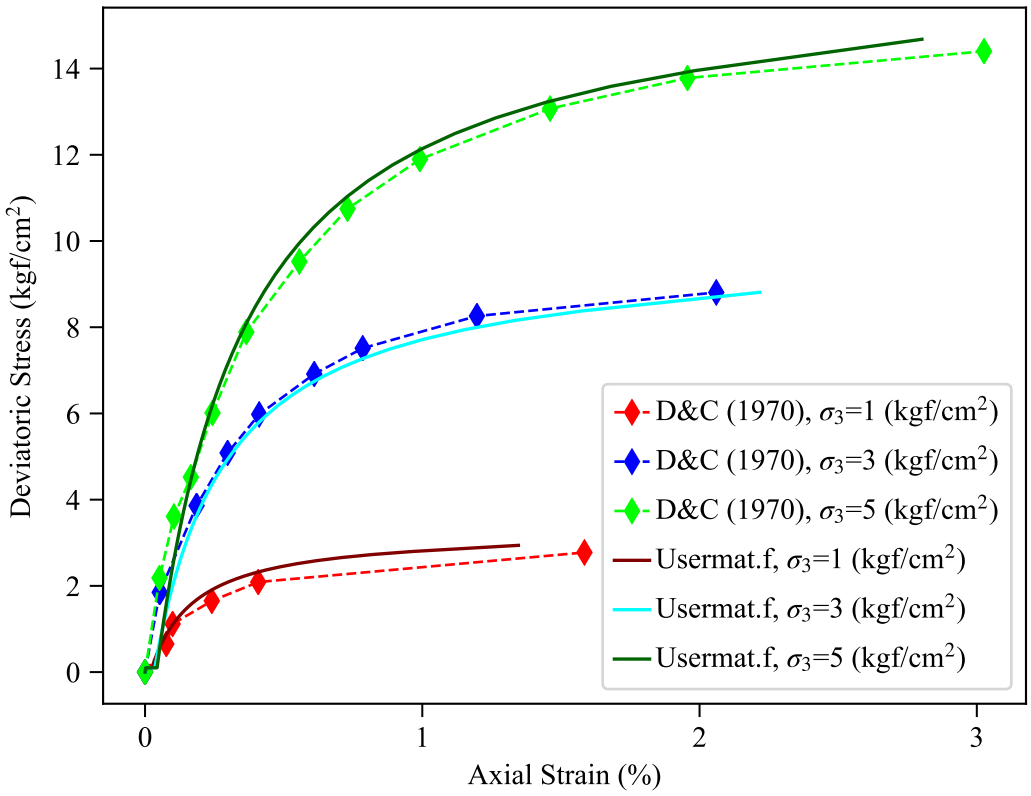

Figure 5.16: ANSYS Usermat.f simulation vs. D&C (1970) triaxial test (dense sand)

soil and pile is modeled with 3D, 8-node surface to surface contact elements. Friction angle is taken as $\delta_s = 21°$.

5.4.1 Verification of Constant Load Amplitude

A horizontal load of 4.0 kN is applied at the top of monopile for 15000 cycles, with a period of 6.3 seconds. Additionally, a static 5.0 kN force is applied vertically to stabilize the system. The design of the model and loading scheme are illustrated in Figure 5.17, test details are shown in 5.18.

As an initial state, the weight of soil is applied by gravity load in which it is analyzed with the linear elastic constitutive relation. In this regard, the coefficient of lateral earth pressure at rest ($k_0 = 1 - sin\phi$) is provided through Poisson's ratio as indicated

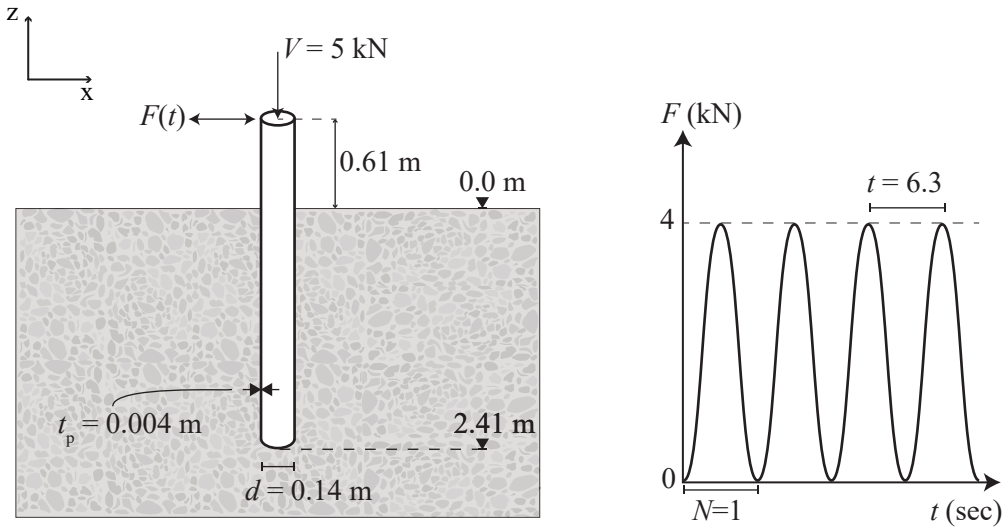

Figure 5.17: Dimension of monopile & loading scheme

in Equation 5.2 [43].

$$\nu = \frac{k_0}{k_0 + 1} \tag{5.2}$$

By taking advantage of symmetrical geometry, the half model is meshed, shown in Figure 5.19. Since the cyclic lateral force is applied in the x-direction, the result of the analysis is plotted for x-component of displacement in Figure 5.20.

Furthermore, the outcome of ECDC is compared with test by Tasan (2011), and methods of API (2000), and Long & Vanneste (1994) [43, 80, 81], in Figure 5.21. API (2000) and Long & Vanneste (1994) state their model based on the p-y method. The p-y method is the most prevalent approach to numerically analyze the piles under the lateral loading, and it utilizes the Beam on Nonlinear Winkler Foundation (BNWF) approach to model the soil-pile interaction [82, 83].

The graph in Figure 5.21 displays the plot of head displacement in x-direction normalized with the pile diameter to the number of loading cycles. Comparison with test indicates ECDC provides improved prediction over these methods for constant amplitude of cyclic loads. Moreover, it over-estimates the test result which is preferable over the under-estimated predictions of API (2000) and Long & Vanneste (1994). Fur-

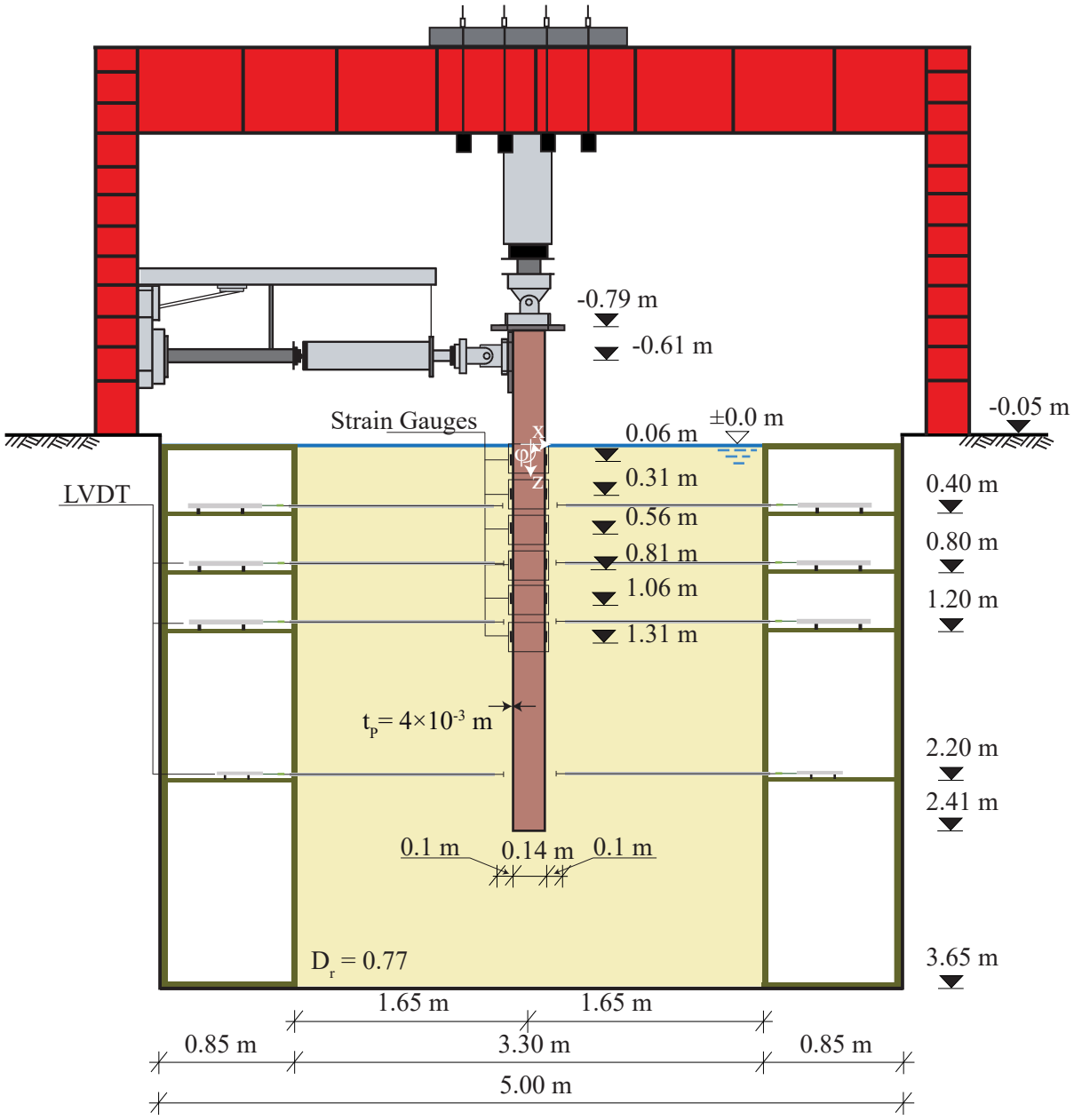

Figure 5.18: Test details of Tasan [43]

thermore, the p-y method of API (2000) and Long & Vanneste (1994) was originally proposed to analyze the pile under monotonic lateral loading. API (2000) achieves the effects of the cyclic loading by a coefficient which reduces the bearing capacity of soil, yet it is independent of the number of load cycles. On the other hand, Long & Vanneste (1994) adjusts the static p-y curve to embody the cyclic loading effect by decreasing soil reaction modulus [81]. The reduction factor is calculated with the

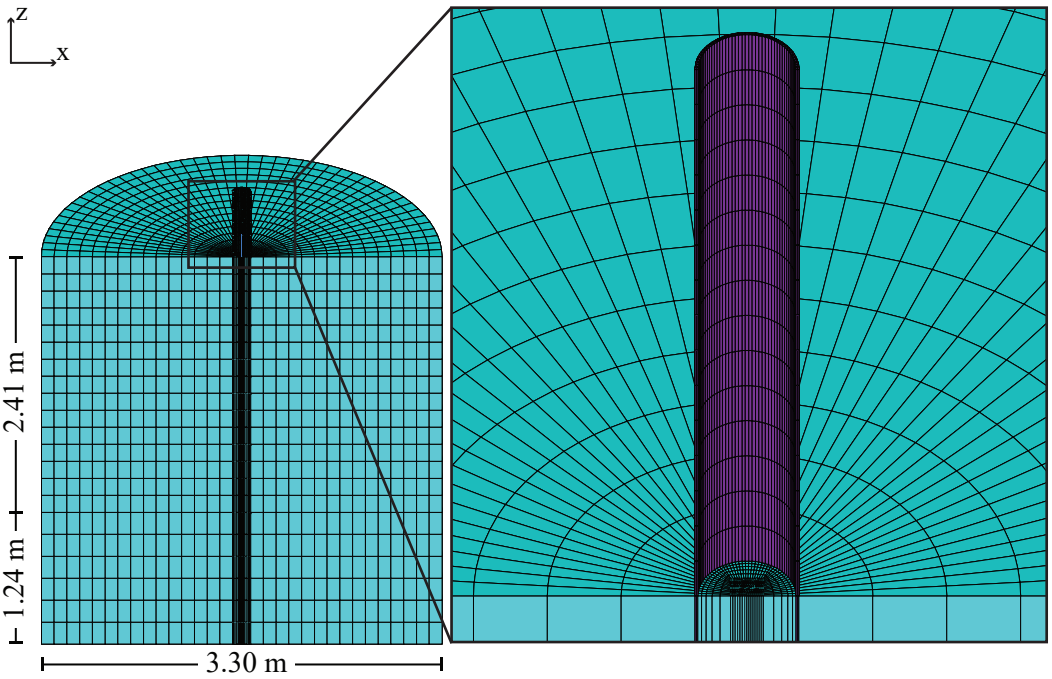

Figure 5.19: 3D meshed model of design

number of load cycles. Nevertheless, this approach works better up to 50 cycles of load [81]. On the contrary, ECDC is a suitable method for both low and high number of loading cycles.

It is important to note that there is no pore-water pressure development in test by Tasan due to its design and loading properties [43]. Excess pore-water pressure may deviates prediction ECDC.

5.4.2 Verification of Varying Load Amplitude

The ECDC model also has the ability to predict deformation caused by cyclic load with varying amplitudes. It utilizes a strain-hardening method to estimates cumulative permanent deformation which is mention in section 4.1.2.2. Recall that in the previous section, a repeated loading $F_{max} = 4.0\ kN$ was applied to a monopile with 15000 cycles. In this section, subsequent to 15000 cycles of $F_{max_1} = 4.0\ kN$, 15000 cycles of $F_{max_2} = 6.2\ kN$ and 15000 cycles of $F_{max_3} = 5.0\ kN$ are applied to the monopile, respectively.

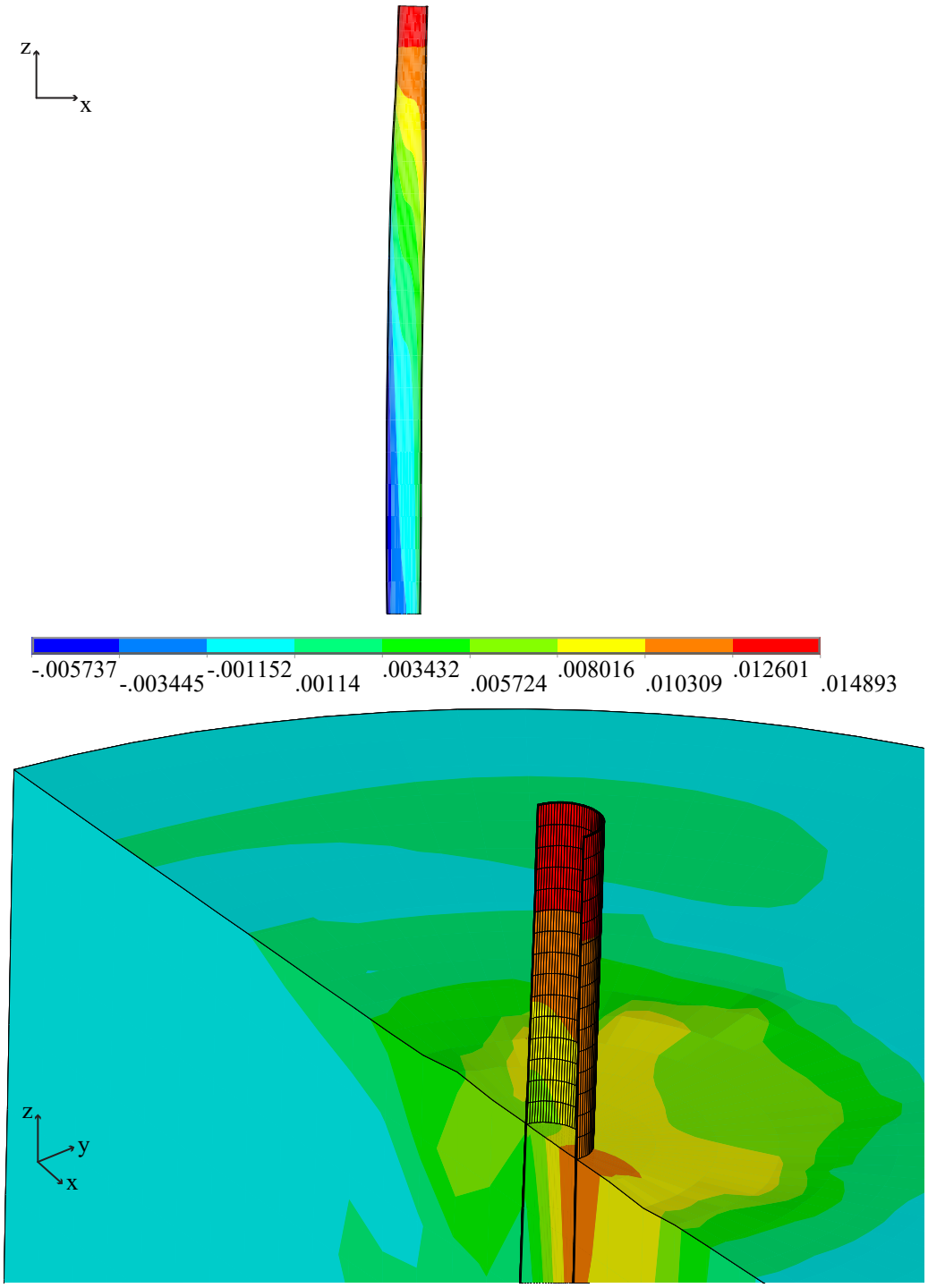

Figure 5.20: x-direction displacement after 15000 cycles

In this regard, the finite element solution using ECDC is presented in Figure 5.22. It provides an improved prediction of the monopile head shift in case of varying load amplitude. For zone 1 (0-15000 cycles, $F_{max} = 4.0\ kN$), ECDC slightly over-

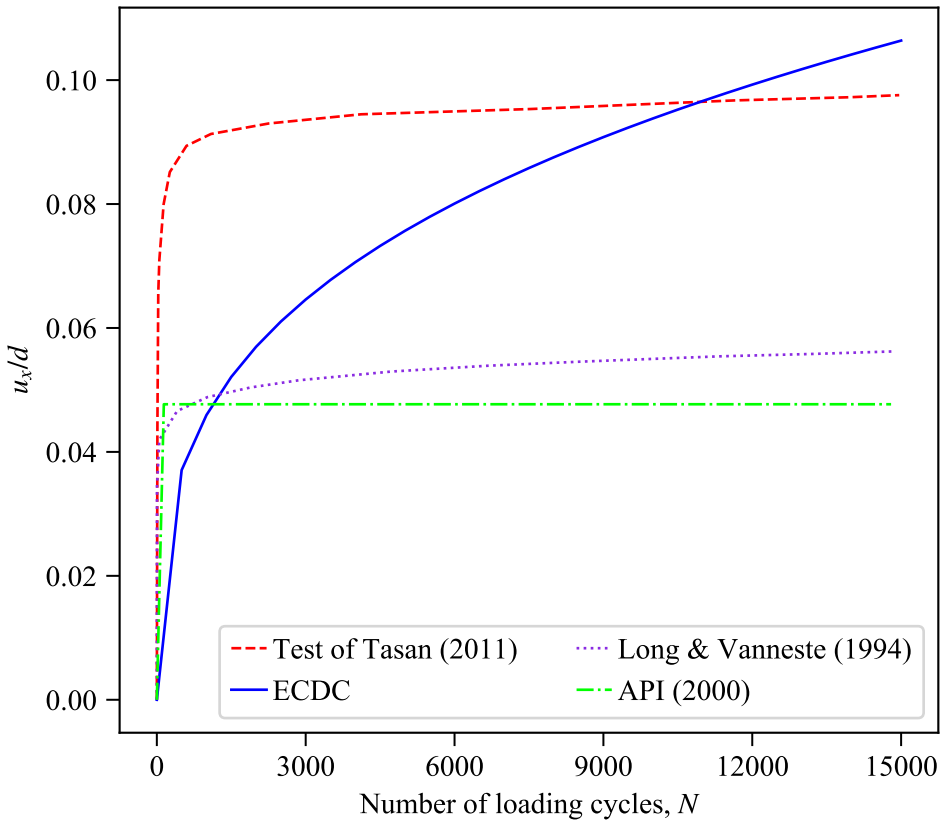

Figure 5.21: Monopile under constant amplitude load

estimates deformations at the end of that zones by 9% whereas for zone 2 (15000-30000 cycles, $F_{max_2} = 6.2\ kN$) and zone 3 (30000-45000 cycles, $F_{max_3} = 5.0\ kN$) it under-estimates deformations. After about 11000 cycles, the deformation estimation of the ECDC intersects with the test result in zone 1. In zone 2, horizontal cyclic loads are higher than the previous zone, and the prediction of ECDC is getting closer across the zone. Zone 3 has a lower horizontal cyclic load than zone 2. The prediction in zone 3 in which deformation estimation does not intersect, under-performs. Overall, the output of ECDC is well aligned with test data throughout a total of 30000 cycles of loading, yet it provides shifted prediction when loading amplitude is decreased.

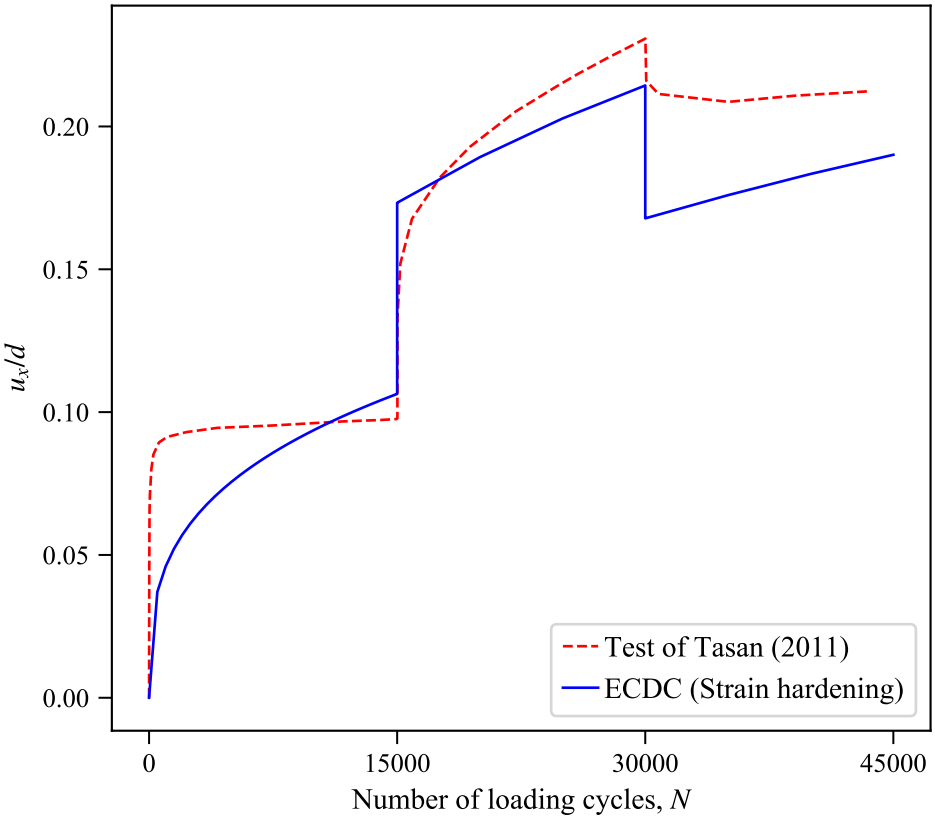

Figure 5.22: Monopile under varying amplitude load

CHAPTER 6

CONCLUSIONS

6.1 Concluding Remarks

This thesis investigated soil behavior under both monotonic and cyclic loading. It provides a simplified approach to calculate permanent deformation of soil from initial state, which is gravitational loading, to final stage, which is the high number of cyclic loading using finite element method. The following can be concluded:

- The outcomes of the monopile analysis indicate that ECDC offers an enhanced prediction of displacement over other methods mentioned in the related section.
- In addition, it provides deformation prediction in the case of varying cyclic load amplitude with strain-hardening method.
- The required parameters for analysis are readily obtainable from several static triaxial and cyclic triaxial tests. ECDC presents a model that involves only two different types of laboratory tests and it requires fewer parameters that are easily derivable to apply for related designs. Moreover, ECDC does not require additional plastic yield surface control like other explicit methods.
- The proposed model can be performed on structures with 3D complex design. It is capable of being implemented not only on a monopile but also to unbound granular materials (UGM) layer of highway pavement or any other case of granular materials subjected to repeated loading.
- Furthermore, another significant advantage of this model is that permanent deformation caused by cyclic loading is computed by explicit approach; thus,

there is no error accumulation due to high number of load cycles. For instance, computational resource and analysis time are equal whether the soil is subjected to a hundred loading cycles or a million cycles.

6.2 Future Perspectives

Beyond the verification process of this study, ECDC can be verified by further experimental tests. In this work, analysis results are compared with experimental tests on poorly graded Berlin sand. Further experimentation on cohesive soil types or well-graded sand can be modeled and verified with ECDC.

One of the main achievements of this model is that it can simulate 3D complex design. Although it has the capacity to calculate the effects of loading with varying directions, only the effects of horizontal load in the x-direction are calculated and then, the results are verified with experimental tests. Cyclic horizontal loading in different directions or cyclic loading with oblique angle can be tested and verified with the proposed model. Moreover, time-hardening method can be implemented and compared with strain-hardening method in the case of varying cyclic load amplitude. In addition to the mentioned possibilities, analysis with different relative density layers and effects of soil-structure interaction can be investigated in depth.

REFERENCES

[1] M. Pastor, A. Chan, P. Mira, D. Manzanal, J. Fernández Merodo, and T. Blanc, "Computational geomechanics: the heritage of Olek Zienkiewicz," *International Journal for Numerical Methods in Engineering*, vol. 87, no. 1-5, pp. 457–489, 2011.

[2] A. Schofield and P. Wroth, *Critical state soil mechanics*, vol. 310. McGraw-Hill London, 1968.

[3] T. Wichtmann, *Explicit accumulation model for non-cohesive soils under cyclic loading*. PhD thesis, Inst. für Grundbau und Bodenmechanik Braunschweig, Germany, 2005.

[4] H. E. Tresca, *Sur l'ecoulement des corps solides soumis á de fortes pressions*. Imprimerie de Gauthier-Villars, successeur de Mallet-Bachelier, rue de Seine, 1864.

[5] R. v. Mises, "Mechanik der festen körper im plastisch-deformablen zustand," *Nachrichten von der Gesellschaft der Wissenschaften zu Göttingen, Mathematisch-Physikalische Klasse*, vol. 1913, pp. 582–592, 1913.

[6] D. C. Drucker, "Relation of experiments to mathematical theories of plasticity," *Journal of Applied Mechanics-Transactions of the ASME*, vol. 16, no. 4, pp. 349–357, 1949.

[7] D. C. Drucker and W. Prager, "Soil mechanics and plastic analysis or limit design," *Quarterly of Applied Mathematics*, vol. 10, no. 2, pp. 157–165, 1952.

[8] K. H. Roscoe, A. Schofield, and a. P. Wroth, "On the yielding of soils," *Geotechnique*, vol. 8, no. 1, pp. 22–53, 1958.

[9] K. Roscoe, A. Schofield, and A. Thurairajah, "Yielding of clays in states wetter than critical," *Geotechnique*, vol. 13, no. 3, pp. 211–240, 1963.

[10] J. M. Duncan and C.-Y. Chang, "Nonlinear analysis of stress and strain in soils," *Journal of Soil Mechanics & Foundations Div*, vol. 5, pp. 1629–1653, 1970.

[11] D. Kolymbas, "An outline of hypoplasticity," *Archive of applied mechanics*, vol. 61, no. 3, pp. 143–151, 1991.

[12] H. B. Seed and R. L. McNeill, "Soil deformations in normal compression and repeated loading tests," *Highway Research Board Bulletin*, no. 141, 1956.

[13] H. B. Seed and C. K. Chan, "Clay strength under earthquake loading conditions," *Journal of Soil Mechanics & Foundations Div*, vol. 92, 1966.

[14] B. Seed and K. L. Lee, "Liquefaction of saturated sands during cyclic loading," *Journal of Soil Mechanics & Foundations Div*, vol. 92, 1966.

[15] G. Sweere, "Unbound granular bases for roads (doctoral thesis)," *Delft University of Technology, Netherlands*, 1990.

[16] F. Lekarp and A. Dawson, "Modelling permanent deformation behaviour of unbound granular materials," *Construction and Building Materials*, vol. 12, no. 1, pp. 9–18, 1998.

[17] S. Werkmeister, A. Dawson, and F. Wellner, "Pavement design model for unbound granular materials," *Journal of Transportation Engineering*, vol. 130, no. 5, pp. 665–674, 2004.

[18] C. Chazallon, P. Hornych, and S. Mouhoubi, "Elastoplastic model for the long-term behavior modeling of unbound granular materials in flexible pavements," *International Journal of Geomechanics*, vol. 6, no. 4, pp. 279–289, 2006.

[19] F. Allou, C. Petit, C. Chazallon, and P. Hornych, "Shakedown approaches to rut depth prediction in low-volume roads," *Journal of Engineering Mechanics*, vol. 136, no. 11, pp. 1422–1434, 2010.

[20] M. J. I. Alam, C. Gnanendran, and S. Lo, "Modelling the settlement behaviour of a strip footing on sloping sandy fill under cyclic loading conditions," *Computers and Geotechnics*, vol. 86, pp. 181–192, 2017.

[21] O. C. Zienkiewicz, A. Chan, M. Pastor, B. Schrefler, and T. Shiomi, *Computational geomechanics*. Citeseer, 1999.

[22] J.-g. Qian, J.-b. Gu, X.-q. Gu, and M.-s. Huang, "Discrete numerical modeling of granular materials considering crushability," *Journal of Mountain Science*, vol. 14, no. 4, pp. 758–770, 2017.

[23] O. C. Zienkiewicz, R. L. Taylor, and J. Z. Zhu, *The finite element method: its basis and fundamentals*. Oxford, UK: Elsevier, 2005.

[24] O. A. Bauchau and J. I. Craig, *Structural analysis: with applications to aerospace structures*, vol. 163. Springer Science & Business Media, 2009.

[25] W. Voigt, *Lehrbuch der kristallphysik*, vol. 962.

[26] S. Goktepe, "Computational inelasticity, lecture notes," Fall 2019.

[27] J. N. Reddy, *Energy principles and variational methods in applied mechanics*. John Wiley & Sons, 2002.

[28] J. Fish and T. Belytschko, *A first course in finite elements*. Chichester, West Sussex, UK: Wiley, 2007.

[29] O. C. Zienkiewicz and R. L. Taylor, *The finite element method for solid and structural mechanics*. Oxford, UK: Elsevier, 2005.

[30] G.-R. Liu and S. S. Quek, *The finite element method: a practical course*. Bristol, UK: Butterworth-Heinemann, 2013.

[31] S. S. Rao, *The finite element method in engineering*. Miami, Florida, USA: Butterworth-Heinemann, 2017.

[32] D. L. Logan, *A first course in the finite element method*. Boston, Mass., USA: Cengage Learning, 2011.

[33] J. M. Duncan, "State of the art: limit equilibrium and finite-element analysis of slopes," *Journal of Geotechnical engineering*, vol. 122, no. 7, pp. 577–596, 1996.

[34] R. L. Kondner, "Hyperbolic stress-strain response: cohesive soils," *Journal of the Soil Mechanics and Foundations Division*, vol. 89, no. 1, pp. 115–144, 1963.

[35] N. Janbu, "Soil compressibility as determined by odometer and triaxial tests," in *Proc. European Conference on SMFE, Wiesbaden, Germany*, vol. 1, pp. 19–25, 1963.

[36] J. Duncan, P. Byrne, K. Wong, and P. Mabry, "Strength, stress-strain and bulk modulus parameters for finite element analyses of stresses and movements in soil masses," *Report No. UCB/GT/80-01*, 1980.

[37] B. M. Das, *Advanced soil mechanics*. London, UK: CRC Press, 2013.

[38] M. Budhu, *Soil Mechanics Fundamentals*. Hoboken, NJ, USA: John Wiley & Sons, 2015.

[39] M. Zytynski, M. Randolph, and C. Wroth, "On Modelling the Unloading-Reloading," *International Journal for Numerical and Analytical Methods in Geomechanics*, vol. 2, no. June 1977, pp. 87–93, 1978.

[40] F. H. Kulhawy and J. M. Duncan, "Stresses and movements in oroville dam," *Journal of Soil Mechanics & Foundations Div*, vol. 98, no. 7, pp. 653–665, 1972.

[41] D. Cathie and R. Dungar, "Evaluation of finite element predictions for constructional behaviour of a rockfill dam.," *Proceedings of the Institution of Civil Engineers*, vol. 65, no. 3, pp. 551–568, 1978.

[42] M. D. Boscardin, E. T. Selig, R.-S. Lin, and G.-R. Yang, "Hyperbolic parameters for compacted soils," *Journal of Geotechnical Engineering*, vol. 116, no. 1, pp. 88–104, 1990.

[43] H. E. Tasan, *Zur Dimensionierung der Monopile-Gründungen von Offshore-Windenergieanlagen*. PhD thesis, Universitätsbibliothek der Technische Universität Berlin, 2011.

[44] F. Lekarp, U. Isacsson, and A. Dawson, "State of the art. ii: Permanent strain response of unbound aggregates," *Journal of Transportation Engineering*, vol. 126, no. 1, pp. 76–83, 2000.

[45] S. Jalbi, L. Arany, A. Salem, L. Cui, and S. Bhattacharya, "A method to predict the cyclic loading profiles (one-way or two-way) for monopile supported offshore wind turbines," *Marine Structures*, vol. 63, pp. 65–83, 2019.

[46] M. Shenton, "Deformation of railway ballast under repeated loading conditions," in *Railroad track mechanics and technology*, pp. 405–425, Elsevier, 1978.

[47] T. Kokusho, T. Hara, and R. Hiraoka, "Undrained shear strength of granular soils with different particle gradations," *Journal of Geotechnical and Geoenvironmental Engineering*, vol. 130, no. 6, pp. 621–629, 2004.

[48] A. Gotschol, "Veränderliche elastisches und plastisches verhalten nichtbindiger böden und schotter unter zyklisch-dynamischer beanspruchung," *Schriftenreihe Geotechnik Universität Kassel, Herausgeber H.-G. Kempfert, Heft 12*, 2002.

[49] C. L. Monismith, N. Ogawa, and C. Freeme, "Permanent deformation characteristics of subgrade soils due to repeated loading," *Transportation Research Record*, no. 537, 1975.

[50] J. Poulsen and R. Stubstad, "Laboratory testing of cohesive subgfrades: Results and implications relative to structural pavement design and distress models," *Transportation Research Record*, no. 671, 1978.

[51] N. Thom and S. F. Brown, *Effect of moisture on the structural performance of a crushed-limestone road base*. No. 1121, 1987.

[52] R. D. Barksdale, "Laboratory evaluation of rutting in base course materials," in *Third International Conference on the Structural Design of Asphalt Pavements, Grosvenor House, Park Lane, London, England, Sept. 11-15, 1972.*, vol. 1, 1972.

[53] A. Dawson, N. Thom, and J. Paute, "Mechanical characteristics of unbound granular materials as a function of condition," *Gomes Correia, Balkema, Rotterdam*, pp. 35–44, 1996.

[54] M. Kamal, A. Dawson, O. Farouki, D. Hughes, and A. Sha'at, "Field and laboratory evaluation of the mechanical behavior of unbound granular materials in pavements," *Transportation Research Record*, pp. 88–88, 1993.

[55] S. Werkmeister, A. R. Dawson, and F. Wellner, "Permanent deformation behavior of granular materials and the shakedown concept," *Transportation Research Record*, vol. 1757, no. 1, pp. 75–81, 2001.

[56] G. Dormon and C. Metcalf, "Design curves for flexible pavements based on layered system theory," *Highway Research Record*, vol. 71, pp. 69–84, 1965.

[57] M. Witczak, "Fatigue subsystem solution for asphalt concrete airfield pavements," in *52nd Annual Meeting of the Highway Research Board, Washington District of Columbia, United States*, no. 140, 1973.

[58] V. A. Diyaljee and G. P. Raymond, "Repetitive load deformation of cohesionless soil," *Journal of the Geotechnical Engineering Division*, vol. 108, no. 10, pp. 1215–1229, 1982.

[59] J. H. Haynes, "Effects of repeated loading on gravel and crushed stone base course materials used in the AASHO road test, final report, joint highway research project, project: C-36-45h, file:6-18-8," tech. rep., 1961.

[60] G. Cerni, F. Cardone, A. Virgili, and S. Camilli, "Characterisation of permanent deformation behaviour of unbound granular materials under repeated triaxial loading," *Construction and Building Materials*, vol. 28, no. 1, pp. 79–87, 2012.

[61] P. Hornych, C. Chazallon, F. Allou, and A. El Abd, "Prediction of permanent deformations of unbound granular materials in low traffic pavements," *Road Materials and Pavement Design*, vol. 8, no. 4, pp. 643–666, 2007.

[62] R. García-Rojo and H. Herrmann, "Shakedown of unbound granular material," *Granular matter*, vol. 7, no. 2-3, pp. 109–118, 2005.

[63] A. Hyde, *Repeated load triaxial testing of soils*. PhD thesis, University of Nottingham, 1974.

[64] G. Gidel, P. Hornych, D. Breysse, A. Denis, *et al.*, "A new approach for investigating the permanent deformation behaviour of unbound granular material using the repeated loading triaxial apparatus," *Bulletin des laboratoires des Ponts et Chaussées*, no. 233, 2001.

[65] D. Li and E. T. Selig, "Cumulative plastic deformation for fine-grained subgrade soils," *Journal of Geotechnical Engineering*, vol. 122, no. 12, pp. 1006–1013, 1996.

[66] H. Kempfert and Y. Hu, "Numerical modeling of the deformation in railway foundation-a case study," in *Proc. 7th Int. Symp. Numer. Models Geomech., Graz*, pp. 669–674, 1999.

[67] R. W. Lentz and G. Y. Baladi, "Constitutive equation for permanent strain of sand subjected to cyclic loading," *Transportation Research Record*, vol. 810, pp. 50–54, 1981.

[68] S. Khedr, "Deformation characteristics of granular base course in flexible pavements," *Transportation Research Record*, vol. 1043, pp. 131–138, 1985.

[69] G. Behzadi and W. Yandell, "Determination of elastic and plastic subgrade soil parameters for asphalt cracking and rutting prediction," *Transportation Research Record*, vol. 1540, no. 1, pp. 97–104, 1996.

[70] M. Huurman, "Development of traffic induced permanent strain in concrete block pavements," *Heron-English Edition*, vol. 41, pp. 29–52, 1996.

[71] H. Wolff and A. Visser, "Incorporating elasto-plasticity in granular layer pavement design," vol. 105, no. 4, 1994.

[72] J. Paute, P. Hornych, and J. Benaben, "Repeated load triaxial testing of granular materials in the french network of laboratories des ponts et chaussées," in *Flexible Pavements. Proceedings of the European Symposium Euroflex 1993 held in Lisbon, Portugal, 20-22 September 1993*, 1996.

[73] O. Zienkiewicz, C. Chang, and E. Hinton, "Non-linear seismic response and liquefaction," *International Journal for Numerical and Analytical Methods in Geomechanics*, vol. 2, no. 4, pp. 381–404, 1978.

[74] A. Niemunis, T. Wichtmann, and T. Triantafyllidis, "A high-cycle accumulation model for sand," *Computers and Geotechnics*, vol. 32, no. 4, pp. 245–263, 2005.

[75] E. Pietropaoli, "Progressive failure analysis of composite structures using a constitutive material model (usermat) developed and implemented in ansys©," *Applied Composite Materials*, vol. 19, no. 3-4, pp. 657–668, 2012.

[76] Ansys, "Ansys mechanical apdl programmer's manual," *Release 14.0*, 2011.

[77] P. A. Allen and C. D. Wilson, "Development of a pressure-dependent constitutive model with combined multilinear kinematic and isotropic hardening," in *ABAQUS Users' Conference*, p. 49, 2004.

[78] J. Desrues, E. Andò, F. A. Mevoli, L. Debove, and G. Viggiani, "How does strain localise in standard triaxial tests on sand: Revisiting the mechanism 20 years on," *Mechanics Research Communications*, vol. 92, pp. 142–146, 2018.

[79] T. J. Hughes, *The finite element method: linear static and dynamic finite element analysis*. Englewood Cliffs, New Jersey, USA: Prentice-Hall, 1987.

[80] API, *2A-WSD, Recommended practice for planning, designing and constructing fixed offshore platforms-working stress design*. Washington, DC, USA: American Petroleum Institute, 2000.

[81] J. Long and G. Vanneste, "Effects of cyclic lateral loads on piles in sand," *Journal of Geotechnical Engineering*, vol. 120, no. 1, pp. 225–244, 1994.

[82] R. Salgado, *The engineering of foundations*. New York, USA: McGraw-Hill, 2008.

[83] C. R. McGann, P. Arduino, and P. Mackenzie-Helnwein, "Applicability of conventional py relations to the analysis of piles in laterally spreading soil," *Journal of Geotechnical and Geoenvironmental Engineering*, vol. 137, no. 6, pp. 557–567, 2010.